

**Project: JB3-CBS2**

**Mechanical, Power, and Thermal Subsystem Design  
for a CubeSat Mission**

A Major Qualifying Project

Submitted to the Faculty

of

WORCESTER POLYTECHNIC INSTITUTE

in partial fulfillment of the requirements for the

Degree of Bachelor of Science

in Aerospace Engineering

by

Joe Bauer

Michael Carter

Kaitlyn Kelley

Ernie Mello

Sam Neu

Alex Orphanos

Tim Shaffer

Andrew Withrow

23 April 2012

Prof. John Blandino, Project Advisor

## **Abstract**

The goals of this Major Qualifying Project (MQP) were the design of thermal, mechanical, and power subsystems for a CubeSat supporting a university-led science mission to orbit an X-ray spectrophotometer. The spacecraft thermal analysis included calculation of unsteady temperature distributions over the course of several orbits. This analysis included radiation from the sun and earth as well as a preliminary analysis of heat generation from internal components. The mechanical design included component and assembly-level, solid models of several spacecraft configurations and a preliminary stress analysis. The power subsystem design included component selection for power generation, management, and distribution as well as energy storage. Additionally, each subsystem team proposed basic experiments in a vacuum chamber that would serve as proof of concept testing and component validation.

## **Acknowledgements**

We would like to extend our thanks to our advisor for his constructive advice and leadership throughout the project.

**Professor John J. Blandino, Ph.D.**

Associate Professor, Aerospace Engineering Program  
Department of Mechanical Engineering, Worcester Polytechnic Institute

Additionally, we would like to thank Profs. Gatsonis and Demetriou and their respective teams for their contributions to the overall CubeSat mission design.

**Professor Nikolaos Gatsonis, Ph.D.**

Director, Aerospace Engineering Program  
Department of Mechanical Engineering, Worcester Polytechnic Institute

**Professor Michael Demetriou, Ph.D.**

Professor, Aerospace Engineering Program  
Department of Mechanical Engineering, Worcester Polytechnic Institute

## **Authorship**

Our project team was divided into three subsystems: mechanical, thermal and power. The team of Joe Bauer, Ernie Mello and Alex Orphanos supplied sections regarding the mechanical subsystem. Michael Carter, Sam Neu and Andrew Withrow created the thermal sections. Kaitlyn Kelley and Tim Shaffer were the authors of the power sections. However, due to the collaborative nature of the MQP, all members were involved in the editing and revision of the project. The final report can be considered a group effort, with multiple partners collaborating on each section.

# Table of Contents

Abstract .....	i
Acknowledgements .....	ii
Authorship .....	iii
Table of Contents .....	iv
Table of Figures .....	vi
List of Tables .....	viii
Executive Summary .....	ix
1. Introduction .....	1
1.1 Project Goals and Objectives .....	1
1.2 Mechanical Structure Subsystem Objectives .....	3
1.2.1 Recreate 3U CubeSat Structural Model for Design and Testing .....	3
1.2.2 Vacuum Chamber Structural Testing .....	3
1.2.3 Mechanical and Structural Support for Other Subsystems .....	4
1.3 Thermal Subsystem Objectives .....	4
1.4 Power Subsystem Objectives .....	5
2. Background .....	6
2.1 CubeSat Specifications .....	6
2.2 Mechanical Subsystem .....	9
2.2.1 2010-2011 WPI CubeSat MQP Recommendations .....	9
2.2.2 Commercially Available CubeSat Structures .....	11
2.2.3 Summary of Structural Design Analysis Approaches .....	15
2.2.4 CubeSat Launch Environment .....	18
2.3 Thermal Subsystem .....	22
2.3.1 2010-2011 WPI CubeSat MQP Recommendations .....	22
2.3.2 Space Thermal Environment .....	23
2.3.3 Spacecraft Thermal Control .....	27
2.4 Power Subsystem .....	31
2.4.1 2010-2011 WPI CubeSat MQP Recommendations .....	31
2.4.2 Determining the Acceptable Load .....	32
2.4.3 Power Management and Distribution .....	33

2.4.4. Battery Management.....	35
2.4.5 Power Fault Management .....	36
3. Methodology.....	38
3.1 Research.....	38
3.2 System Engineering Group.....	39
3.3 Mechanical Design and Structural Analysis.....	39
3.3.1 Flight Option Baseline CAD model.....	39
3.3.2 Mechanical and Structural Subsystem Support .....	42
3.3.3 Vacuum Chamber Structural Testing.....	43
3.4 Thermal Analysis.....	46
3.4.1 Modeling of External Components.....	46
3.4.2 Modeling of Internal Components.....	57
3.4.3 Laboratory verification of COMSOL model .....	58
3.5 Power Analysis .....	61
3.5.1 Power Budget.....	61
3.5.2 Baseline System Analysis .....	62
3.5.3 Lab Option Solar Cell Baseline Testing .....	64
4. Analysis and Findings.....	68
4.1 Mechanical Subsystem.....	68
4.2 Thermal Subsystem.....	71
4.2.1 Steady-State Heating in COMSOL.....	72
4.2.2 Multiple Orbits in COMSOL.....	76
4.2.3 Internal Components.....	81
4.2.4 Lab Option Verification.....	88
4.3 Power Subsystem .....	91
5. Conclusions and Recommendations .....	94
5.1 Mechanical Subsystem Conclusions and Recommendations .....	94
5.2 Thermal Subsystem Conclusions and Recommendations .....	97
5.3 Power Subsystem Conclusions and Recommendations.....	98

## Table of Figures

Figure 1 - The P-POD System [39].....	7
Figure 2 - CubeSat Specifications [4].....	8
Figure 3 - Monoblock Design 1 [2] .....	10
Figure 4 - Monoblock Design 2 (Assembly with Subsystem Components from 2010-2011 MQP) [2].....	11
Figure 5 - 3U Skeletonized CubeSat Structure Offered by CubeSat Kit (left) [6], and 2U Structure Offered by ISIS (right) [7] .....	13
Figure 6 - Frequency Profile of GSFC-STD-7000 [5].....	16
Figure 7 - Random Vibration Profile for Various CubeSat Launch Vehicles [19] .....	21
Figure 8 - Effective Emittance vs. Number of Aluminized Layers for Multi-Layer Insulation [17].....	23
Figure 9 - Space Thermal Environment [21] .....	24
Figure 10 - Altitude vs. Visibility Factor $F$ [17].....	25
Figure 11 - Current-Voltage Curve [27] .....	33
Figure 12 - Vacuum Chamber Test Fixture Structure .....	44
Figure 13 - Dimensioned Drawing of Caps .....	45
Figure 14 - Vacuum Chamber Test Fixture with CubeSat and Fine Adjustment Device. ....	45
Figure 15 - COMSOL Mesh of the CubeSat .....	48
Figure 16 - Tests with Thermally Resistive and Conductive Layers.....	49
Figure 17 - Selecting the Boundaries for Highly Conductive Layers.....	53
Figure 18 - Analytic Function to Vary the Solar Flux over 10 Orbits .....	55
Figure 19 - CubeSat Model for Lab Option.....	59
Figure 20 - Vacuum Chamber to be used for Testing the Lab Option .....	60
Figure 21 - Power Management and Distribution Architecture Block Diagram .....	63
Figure 22 - Solar Cell Test Circuit Diagram.....	65
Figure 23 - Solar Cell Testing In Progress.....	66
Figure 24 - I-V Curve for a Single Solar Cell.....	66
Figure 25 - Lab Option Solar Array.....	67
Figure 26 - Von Mises Stress Output Based on Worst Case Frequency Curve.....	69
Figure 27 - Deformation Output Based on Worst Case ASD Curve (x40000 scale) .....	70
Figure 28 - Deformation Output Based on Worst Case ASD Curve .....	71
Figure 29 - Simplified CubeSat Structure.....	72
Figure 30 - Solver Errors .....	73
Figure 31 - Successful Meshing of the Simplified CubeSat Model.....	74
Figure 32 - Steady-State Thermal Model.....	75
Figure 33 - Variation of the Solar Flux vs. Time in MATLAB.....	76
Figure 34 - Temperature Data vs. Time for 10 Orbits .....	78
Figure 35 - Thermal Envelope for External Satellite Components.....	79
Figure 36 - Temperature Distribution (in degrees Kelvin) during Full Illumination .....	80

Figure 37 - Temperature Distribution (in degrees Kelvin) during Eclipse.....	80
Figure 38 - Thermal Analysis of the Stack .....	84
Figure 39 - Thermal Analysis of the GPS.....	85
Figure 40 - Thermal Analysis of the Magnetorquer .....	86
Figure 41 - Thermal Analysis of the Payload .....	87
Figure 42 - LabView VI Front Panel .....	89
Figure 43 - LabView VI Block Diagram .....	89
Figure 44 - Basic Vacuum Chamber CAD Model.....	90
Figure 45 - Temperature of CubeSat during Simulated Cryopump Operation.....	91
Figure 46 - Test Fixture .....	94
Figure 47 - Configuration of Threaded Rod .....	95
Figure 48 – Top View of Connecting Adapters.....	96
Figure 49 - Bottom View of Connecting Adapters.....	96
Figure 50 - Power System Flow Cartoon.....	99



## List of Tables

Table 1 - Generalized Random Vibration Test Levels Components (STS or ELV) 22.7-kg (50-lb) or less [5] .....	16
Table 2 - Typical Launch Loads of Past CubeSat Launch Vehicles [18].....	20
Table 3 - Planetary Albedo Values [23] .....	26
Table 4 - Component Power Demands .....	62
Table 5 - Component Materials .....	81
Table 6 - Internal Components .....	83

## **Executive Summary**

In 2010, WPI joined many universities participating in the CubeSat program. Developed by California Polytechnic State University (San Luis Obispo, CA), the program gives guidelines for designing a miniaturized satellite. WPI began to explore this program in 2010 with the design of a CubeSat structure intended to house an infrared spectrometer [2]. The 2011 project team has expanded this project by partnering with the Space Research Center, Polish Academy of Sciences (Wroclaw, Poland) and the NASA Goddard Space Flight Center (Greenbelt, MD) to design a CubeSat to house an instrument developed by the Polish Academy of Sciences.

The 2011 CubeSat project teams were charged with designing the CubeSat according to specifications of the instrument. The major design constraints were a polar orbit, a tracking system that could pinpoint the sun with a high degree of accuracy, and a high power requirement to run the instrument. Three different MQP teams were responsible for designing the CubeSat under these constraints. The Design and Analysis for a CubeSat Mission report [36] explains instrument selections and basic orbital analysis. The Attitude Determination and Control Design for a CubeSat Mission report [37] discusses the systems employed to control the CubeSat through de-tumble and pointing maneuvers. This report details the contributions of the mechanical, thermal and power subsystems.

In the following report, we outline the basic design for the mechanical, thermal and power subsystems of the CubeSat design. Using tools like COMSOL and SolidWorks, we performed analysis of possible designs. We also constructed additional components for the 2010 MQP team's "Lab Option," a simplified CubeSat model

constructed and tested at WPI. Our baseline design and additions to the Lab Option design provide a foundation for continuing CubeSat projects at WPI.

# 1. Introduction

## 1.1 Project Goals and Objectives

Although designing and launching a satellite is a cornerstone of aerospace engineering, the design process was often inaccessible to college students until the CubeSat program was established. Developed by California Polytechnic State University (Cal Poly) (San Luis Obispo, CA) and Stanford University's Space Systems Lab, the CubeSat program has allowed undergraduate students to gain valuable experience in designing and launching their own picosatellites<sup>1</sup>. Each CubeSat must meet standardized design guidelines before being launched in a standard deployment system, the P-POD [1]. These guidelines provide practical and fairly inexpensive satellite design opportunities to undergraduate and graduate students. With over 60 universities in multiple nations participating in the program [1], CubeSat has been a successful method for allowing college students to access space.

Worcester Polytechnic Institute (WPI) recently initiated development of its own CubeSat in 2010 under the guidance of Professors Gatsonis, Blandino and Demetriou. The Aerospace Engineering program's first CubeSat related MQP project explored the potential of the CubeSat program at WPI [2]. This team of eleven fourth-year undergraduates created an initial design and provided recommendations for future teams. Our project, built upon the foundation of the previous year's work, was composed of fifteen fourth-year undergraduates divided into three subgroups, each headed by a faculty advisor. This report details the work of the Mechanical, Thermal and Power Subsystem,

---

<sup>1</sup> Picosatellites are the smallest type of miniaturized satellites or microsatellites.

which was advised by Professor Blandino. The other groups involved in this project included the Attitude Determination and Control and the Mission Analysis group.

Unlike the previous WPI team's evaluative project, this project involved designing a CubeSat for specific requirements. WPI partnered with a team including scientists from the Space Research Center, Polish Academy of Sciences (Wroclaw, Poland) and the NASA Goddard Space Flight Center (Greenbelt, MD) to design a CubeSat mission to support an x-ray spectrophotometer<sup>2</sup>. Our project team designed a CubeSat based upon this specific instrument's requirements, in addition to the standardized CubeSat guidelines. As the initial design team, our group used specialized analysis tools, such as COMSOL (COMSOL Multiphysics Burlington, MA), SolidWorks (Dassault Systems SolidWorks Corp. Waltham, MA) and Satellite Tool Kit (STK) (AGI Exton, PA) to evaluate and improve our designs. We also conducted preliminary testing with a "Lab Option" structure and solar panel to assess our analytical results.

Our final product, a preliminary CubeSat design to support the x-ray spectrophotometer, is the first step in the CubeSat deployment process. Future groups can use this project team's published conclusions and recommendations to prepare for assembly, testing, and launch of the CubeSat.

---

<sup>2</sup> The instrument is called the SphinX Next Generation (S-NG) soft X-ray spectrophotometer.

## **1.2 Mechanical Structure Subsystem Objectives**

### **1.2.1 Recreate 3U CubeSat Structural Model for Design and Testing**

The original objective for the Mechanical and Structural Subsystem team was to recreate the original (2010) MQP team's SolidWorks model of the 3U CubeSat Structure. This meant updating the structure every time there were design changes, adapting a model with meshing capabilities to allow other subsystem teams to run simulations and tests, and keeping an up-to-date parts and assembly directory. To accompany the structural testing, we performed stress analysis of the structure through SolidWorks Express to provide appropriate data on expected launch loads.

### **1.2.2 Vacuum Chamber Structural Testing**

The CubeSat Lab Option model was assembled last year using computer-aided manufacturing (CAM) software as well as WPI's computer numerical controlled (CNC) machine tools located in Washburn Labs. This structure was intended to enable both hardware and software testing in a vacuum chamber using a one-degree-of freedom rotational test fixture. There were two fixture choices: an open ball bearing and a mount clip for the top and bottom of the structure attached with a filament cable. The choice for open ball bearings came from the lack of lubrication to reduce friction during movement, which is important in a vacuum because most solid or liquid lubricants will outgas and prevent proper testing. The mount clip and torsional filament used with the test stand could create the same effects as the open ball bearings. The Lab Option structure would be put under purely thrust loads and no axial loads during testing. While in orbit, the CubeSat can be considered under no loads since the gravitational acceleration is balanced by the centrifugal acceleration. The vacuum chamber testing on the Lab Option structure can be simplified by applying purely thrust loads.

### **1.2.3 Mechanical and Structural Support for Other Subsystems**

Lastly, using the technical expertise gained during background research, the final objective was to help other subsystems with structural hardware design, simulation test modeling and part design and placement as needed. This was done through the integrated 3U computer aided design (CAD) model that was designed for two sets of conditions: a) one to represent the “full” design and show part placement so as to act as a guide for future changes, and b) the other as a simulation driven model which has been de-featured to allow meshing by the various software tools used to model and test the CubeSat under many different conditions, e.g. COMSOL or SolidWorks Express. Therefore, each group could investigate certain problems by performing specially designed simulations. Also, design decisions could be made regarding the placement, size, mass, and configuration of each part and the assembly as a whole.

### **1.3 Thermal Subsystem Objectives**

The thermal design of a satellite is very important to ensure the health and longevity of a spacecraft in earth orbit. The objectives of the Thermal Subsystem group were to investigate the thermal space environment for our CubeSat’s orbit and any potential conditions it might encounter. Once we determined the conditions it will meet, we need to determine the survivability and operational temperature limits of every component of the CubeSat. To do this, we performed a thermal analysis of a finite element model of the CubeSat using COMSOL to determine how heat will propagate through the structure, and which areas will require attention. Lastly, we sought to investigate feasibility and design thermal control systems to ensure that no components fall outside of the survivable or operational ranges.

## **1.4 Power Subsystem Objectives**

Power systems are vital to producing, storing and distributing power to the various systems on a satellite. To this end, the power subsystem team had four primary objectives. First, the team was responsible for determining the power generated throughout the satellite's orbit. This included analyzing the placement of solar panels, determining the effects of the orbit on satellite illumination and using STK to provide data for power at a given time. Second, the team was responsible for developing a power budget. The team kept records for each component's power demands and proposed a system to keep each component powered as necessary. Third, the team was responsible for developing the Power Management and Distribution (PMAD) architecture to outline the overall power and data flow throughout the satellite's systems. This PMAD system was responsible for any conditioning, distribution and handling of power throughout the satellite. The team researched how the various components within the satellite interfaced with one another and where power would be required and delivered. Finally, the team was also responsible for selecting and mapping power management components from vendors.



## **2. Background**

### **2.1 CubeSat Specifications**

CubeSats were originally developed as a result of a project-based learning experiment at Stanford University in 1994 to study microsattellites [3]. The first CubeSats were launched in 1994 and 1995, and due to their success, Cal Poly and Stanford formed a relationship to educate and assist other student groups in building microsattellites.

Today, CubeSats have become a popular way for universities and other entities to launch a cost-effective satellite. Standardized specifications were created in order to maintain the relatively low cost and simplicity of launching a CubeSat.

The basic CubeSat design specifications ensure the safety of the launch vehicle, CubeSat, and any other CubeSats piggybacking on the mission. The goal is to ensure that if a CubeSat were to fail as a result of a poor or incompatible design choice, it would not cause a failure of the entire launch system [4]. As a result, Cal Poly's specifications require safe deployment from the Poly Picosatellite Orbital Deployer (P-POD), a standardized, Cal Poly designed, CubeSat deployment system. The P-POD has a set of rails on which the CubeSat rests, and uses spring force to launch CubeSats once they are ready for deployment. The specification sheet also notes that no part of the CubeSat is to touch the P-POD aside from the rails.

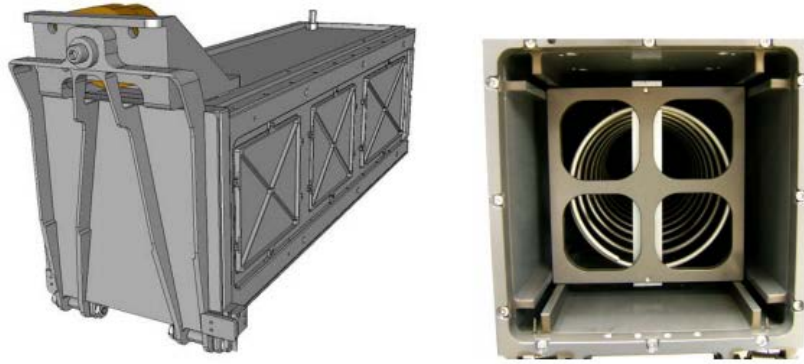


**Figure 1 - The P-POD System [39]**

The basic dimensional specifications of the CubeSat state that the satellite is not to exceed 100mm on the short sides, and 113.5mm per “U” (long side), or unit. The 113.5mm length includes the rails that must be integrated into the P-POD. Without the rail protrusion, the CubeSat height cannot exceed 100mm (see Figure 2). CubeSats may be up to 3U long, or 300mm + 13.5mm for the rail protrusion. The mass of a 3U CubeSat is not to exceed 4kg, making the maximum mass of a 1U CubeSat 1.33kg. Important to note is that the CubeSat center of gravity should not be more than 2cm from the geometric center. Cal Poly restricts the choice of aluminum for the structure and rails to Aluminum 7075 or 6061<sup>3</sup>, with any other choices requiring a special waiver process. More in depth specifications can be found on the Cal Poly Specification sheet shown in Figure 2 [4].

---

<sup>3</sup> Aluminum 7075 is very similar to 6061, where 7075 is made with zinc and can be made to be stronger than 6000 series aluminum.

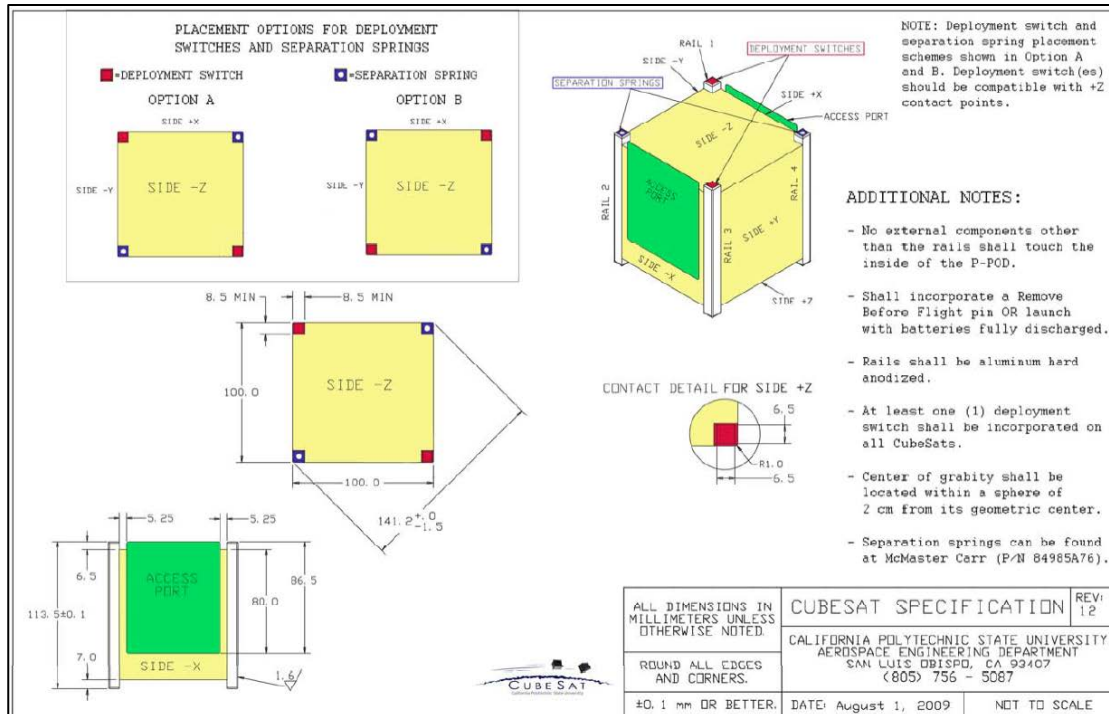


**Figure 2 - CubeSat Specifications [4]**

The waiver process is important for any CubeSat developers whose design choices violate a required specification or guideline. Cal Poly specifically states that the waiver is meant to facilitate communication between the builder of the CubeSat and all other potential handlers, such as the launch operators and the personnel responsible for integrating the CubeSat and P-POD [4]. This process allows a designer to violate the CubeSat specifications if they must do so, and ensures that any outside handlers of the CubeSat have sufficient warning to modify any systems based on these changes.

CubeSats also have numerous electrical requirements during launch. The specifications state that CubeSats must not have any electronics powered up during the launch process [4]. This prevents any possible interference with the launch vehicle or other CubeSats. This also includes having batteries deactivated or discharged prior to launch. CubeSats are also required to have a switch installed in them that will be

depressed while in the P-POD, allowing the designer to have the CubeSat charge batteries and run diagnostics during launch. In addition to these requirements, the specifications call for a Remove Before Flight pin that can be installed on CubeSats which cuts power until the satellite is situated in the P-POD prior to launch, should a CubeSat launch without the batteries discharged [4].

The final part of the specifications outlines the testing a CubeSat must go through. Testing is mandated to ensure that the CubeSat will be safely deployed from the P-POD without incident. The six phases of testing are Random Vibration, Thermal Vacuum Bakeout, Visual Inspection, Qualification, Protoflight, and Acceptance [4]. The specifics of these tests are outlined by the provider of the launch vehicle. The CubeSat specification sheet notes that in the case of an unknown launch provider, there is a basic standard called GSFC-STD-7000, or the General Environmental Verification Standard. This document can be found on the National Aeronautics and Space Administration (NASA) website for further investigation [5].

## **2.2 Mechanical Subsystem**

### **2.2.1 2010-2011 WPI CubeSat MQP Recommendations**

In their final report the 2010-2011 WPI CubeSat Mechanical Subsystem team recommended that future groups use a monolithic design called “Monoblock Design 1” for the primary structure, shown in Figure 3. They concluded that “This type of design requires the least amount of assembly for the structure, which can significantly reduce the overall weight.” They added: “WPI’s machining capabilities cannot support the complex design of a monolithic structure, so the machining will have to either be outsourced to

more capable facilities, or a prefabricated CubeSat structure will have to be purchased from a specialized company such as ISIS or Pumpkin” [2].

The 2010-2011 MQP team also suggested a design which they called “Monoblock Design 2” should be considered for the primary structure in future projects. They noted that it “has a similar appearance in structure to the CubeSat Kit model” and “the walls consist of a cross lattice design in order to optimize mass and structural integrity” [2]. Monoblock Design 2 is shown in Figure 4.

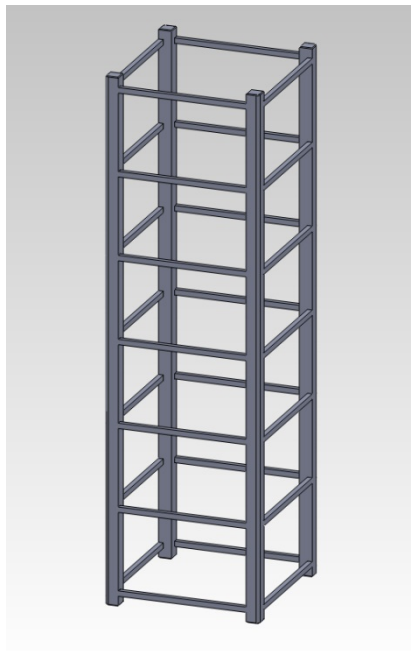


**Figure 3 - Monoblock Design 1 [2]**



**Figure 4 - Monoblock Design 2 (Assembly with Subsystem Components from 2010-2011 MQP) [2]**

### **2.2.2 Commercially Available CubeSat Structures**

When selecting the framework for a CubeSat, developers can turn to companies that specialize in the prefabrication of standardized, commercially available CubeSat structures and components [2]. In today's market, with respect to CubeSat flight heritage, there are two companies stand out: Pumpkin Incorporated (Pumpkin) (San Francisco, CA) and Innovative Solutions in Space (ISIS) (Delft, Netherlands). Both companies sell sets of CubeSat structural components which adhere to the CubeSat specifications created by Cal Poly and Stanford University. Once received, these components must then be assembled by the developer [2].

Pumpkin, which refers to its CubeSat-related products as “CubeSat Kits”, regards itself as the “de facto standard in the CubeSat universe” and provides the most space-proven CubeSat structural components [6]. As noted on their website, the design

approach of Pumpkin’s structural components is based “specifically on several interdependent aspects of structural design” [6]. The company delivers kits to developers which contain all the components necessary for a relatively short and inexpensive assembly.

In the aerospace industry, flight heritage is often a deciding factor in the component selection process. The CubeSat Kit design is in its fourth generation and has been delivered to more than 150 customers since 2003 [6]. The flight heritage of its 1U and 3U structures alone is unsurpassed in the CubeSat domain, as they have together been part of at least seven different CubeSat missions which have flown in space since 2007 [6]. In addition, Pumpkin offers downloadable CAD files of their completed structures and individual components in various software versions. Although these files generally need to be de-featured<sup>4</sup> in order to run test simulations in software packages such as COMSOL or SolidWorks Simulation, they still serve as valuable starting points from which computer-aided alterations can be made.

The primary Pumpkin structure consists of six chassis walls made of 5052-H32<sup>5</sup> hard-anodized<sup>6</sup> and alodined<sup>7</sup> sheet aluminum. The walls are fastened together with ten, M3 x 5mm non-magnetic stainless steel flathead screws [6]. For mass reduction, Pumpkin also offers a “skeletonized” chassis wall design, which features various cut-outs in the six structural panels. Both designs are covered with a cover plate assembly, which

---

<sup>4</sup> Complex CAD drawings with large amounts of small features can cause problems when software packages such as SolidWorks or COMSOL try to mesh the drawing to perform simulations.

<sup>5</sup> *5052-H32 Aluminum* – a common sheet metal that has moderate to high strength aluminum manganese alloy. Strain hardened and stabilized, it has good welding characteristics and high resistance to corrosion.

<sup>6</sup> *hard-anodizing* – a process in which aluminum is bathed in sulfuric acid which a low-voltage electric current in order to increase the durability and hardness of aluminum.

<sup>7</sup> *alodining* – the chemical application of a protective chromate conversion coating on aluminum to create a corrosive resistance and electrically conductible surface.

encloses the chassis wall outer-surface and is made from approximately 1.5mm thick sheets of 5052-H32 aluminum. For adaptability, this cover plate assembly is designed to be compatible with a wide variety of subsystem components and payloads specific to the developer’s mission. No deviation waiver needs to be submitted for using Al 5052-H32, since the CubeSat Kit design is already preapproved. All other components are made from 6061-T6 aluminum. The approximate mass of the primary 1U CubeSat structure is 241g, which would yield a structural mass fraction of 0.18 if the total CubeSat mass was maximized. The skeletonized model reduces the overall mass by 85g (39.7%). The cost of a complete 1U solid wall CubeSat structure from CubeSat Kit is about \$1,725 (USD); while a complete 3U solid wall assembly costs about \$3,150 [2]. A model of the “skeletonized” 3U structure from Pumpkin is shown in Figure 5.



**Figure 5 - 3U Skeletonized CubeSat Structure Offered by CubeSat Kit (left) [6], and 2U Structure Offered by ISIS (right) [7]**

Innovative Solutions in Space (ISIS) describes itself as “a company which specializes in [the] miniaturization of satellite systems, with a particular emphasis on the



design and development of subsystems for micro- and nanosatellites” [7]. Specifically, ISIS offers “generic primary satellite structures based on the CubeSat standard” [2]. Although the company has yet to have one of its CubeSat structures flown in space, their website (last updated in 2011) notes that there are “multiple units slated for launch in the upcoming 12 months” [7].

Compared to the CubeSat Kit design, the ISIS structure is much less complex. In contrast to the monoblock design<sup>8</sup> approach taken by Pumpkin, ISIS structures feature a modular design which involves the assembly of multiple smaller components. A 1U structure consists of two modular side frames which are connected to four ribs by M2.5 x 6mm screws. The ISIS structure also contains a secondary structure, which incorporates a circuit board stack to enhance the structural integrity of the satellite [2]. The combined mass of the complete 1U structure is 200g, while the cost is \$3,100 [7]. Figure 5 shows a 2U model CubeSat from ISIS with both primary and secondary structures included.

In contrast to the commercially available option, a large number of CubeSat structures have been independently built or custom-designed to meet the needs of specific missions [2]. These structures are often built at universities or organizations and encompass a variety of designs which differ significantly from those provided by ISIS and Pumpkin [6-10]. These differences can be due to a number of reasons including limited budgets and/or manufacturing capabilities [2].

---

<sup>8</sup> Entire walls created from a single piece of aluminum.

### 2.2.3 Summary of Structural Design Analysis Approaches

There are a few types of loads and stresses mentioned in the GSFC-STD-700, including random vibration, structural loads, sine vibration and mechanical shock. The analysis that is most critical and most physically taxing to the structure of a CubeSat is the random vibrational analysis which ensures the structure survives the launch and can be ejected from the launch vehicle safely. The von Mises stress, a general stress term calculated from the stress tensor of a material at a given time, and structural deformation are important considerations in the vibrational analysis. A material starts to deform when the von Mises stress reach the yield strength of the material. The Cal Poly CubeSat Specifications state that:

#### “3. Testing Requirements

Testing shall be performed to meet all launch provider requirements as well as any additional testing requirements deemed necessary to ensure the safety of the CubeSats and the P-POD. If launch vehicle environment is unknown, GSFC-STD-7000 shall be used to derive testing requirements.” [4]

In addition to the GSFC-STD-700 requirements, the launch vehicle (LV) provider may require additional testing. [4]

Table 1 and Figure 6 show the frequency profile for a worst-case scenario for the acceleration spectral density from the GSFC-STD-7000 document titled *General Environmental Verification Standard (GEVS) for GSFC Flight Programs and Projects* from NASA which details the requirements for CubeSats to be able to survive the launch. When performing a random vibrational analysis, the CubeSat must be able to pass a worst-case scenario test for its own safety and the safety of the launch vehicle. Therefore any analysis software to be considered for our random vibration analysis must allow the user to input the force as a (non-constant) function of frequency.

**Table 1 - Generalized Random Vibration Test Levels Components (STS or ELV)  
22.7-kg (50-lb) or less [5]**

Frequency (Hz)	ASD Level ( $g^2/Hz$ )	
	Qualification	Acceptance
20	0.026	0.013
20-50	+6 dB/oct	+6 dB/oct
50-800	0.16	0.08
800-2000	-6 dB/oct	-6 dB/oct
2000	0.026	0.013
Overall	14.1 $G_{rms}$	10.0 $G_{rms}$

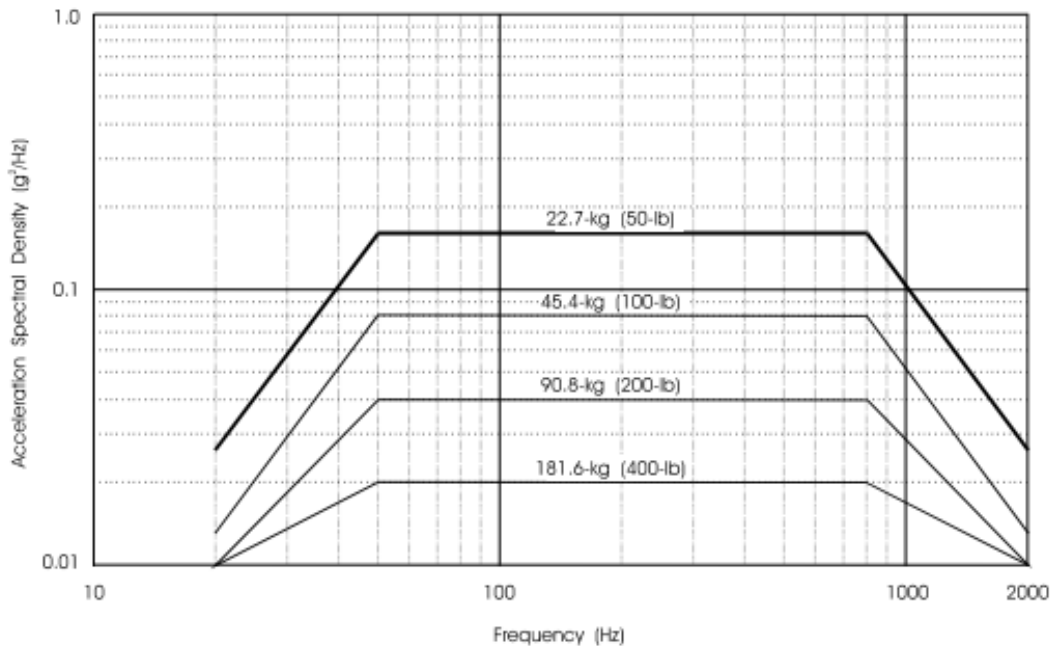


**Figure 6 - Frequency Profile of GSFC-STD-7000 [5]**

We considered three different tools for performing structural analysis on the CubeSat: SolidWorks, NASTRAN (MacNeal-Schwendler Corporation Santa Ana, CA), and ANSYS (ANSYS Inc. Canonsburg, PA). We researched each program’s capabilities and limitations. Our research primarily consisted of choosing a program that had the ability to do random vibration analysis.

ANSYS is capable of both structural static analysis and transient dynamic analysis. Transient dynamic analysis is used to determine the response of a structure under the action of any general time-dependent loads. ANSYS calculates the time varying values of displacement, strain, stress, and force as the simulated structure responds to any combination of static, transient, and harmonic loads [11]. ANSYS is capable of three different solution methods: full, mode-superposition, and reduced. A full solution uses full system matrices, meaning there is no matrix reduction, to calculate transient responses, so there is no matrix reduction, and allows all types of nonlinearities. Mode-superposition sums factored mode shapes and accepts modal damping, but the only nonlinearity allowed is simple node-to-node contact defined by a gap condition. Reduced is a much simpler way to do the analysis, but much more constrained. In the reduced solution method, no nonlinearity is allowed, the time step must be constant, and element loads cannot be applied (e.g. pressures and temperatures) [12].

NASTRAN is a finite element analysis program that was originally developed for NASA in the late 1960s under United States government funding for the aerospace industry [13]. All input and output to the program is in the form of text files. However, multiple software vendors market pre- and post-processors designed to simplify building a finite element model and analyzing the results. These third-party software tools include functionality to import and simplify CAD geometry, mesh with finite elements, and apply loads and restraints [14]. In NASTRAN, random analysis is treated as a data reduction procedure that is applied to the results of a frequency response analysis. The frequency response analysis is performed for sinusoidal loading conditions, each a separate subcase, at a sequence of frequencies. The results are outputted, and at this point “MSC Random”

is used throughout the interface to perform calculations of random responses such as auto and cross power spectral densities and auto and cross correlation functions for all of the result data [15]. The output request for a random response can only be made through the XYOUT module, which is a manual user input of entries and restraints. This creates a burden on a user to prepare XYPLOT or XYPRINT entries for each degree of freedom for nodal responses, and for each stress/force component for element responses. For any size model, a user has to prepare a large number of XYPLOT/XYPRINT entries [16].

SolidWorks is capable of many different analyses including, but not limited to, static, frequency, linear dynamic, harmonic, and random vibration. Random analysis in SolidWorks requires the force, material type, fixtures, global damping, minimum frequencies, maximum frequencies, and frequency profiles to be defined. SolidWorks has a built in library of materials the user can select from, and is relatively easy to use compared to ANSYS and NASTRAN. SolidWorks can output von Mises stress, displacement (deformation), velocity, and acceleration from random vibration analysis data. Due to our group's familiarity with SolidWorks, as well as its relatively easy to use interface, we chose to do our random vibrational analysis in SolidWorks.

#### **2.2.4 CubeSat Launch Environment**

For most spacecraft, including CubeSats, the greatest force loading occurs during the launch. Thus, when conducting virtual or physical tests on a satellite to determine whether or not the spacecraft is ready for the expected mission environment, developers place a great deal of importance on the *launch environment*. During liftoff, static loads are applied along the longitudinal axis of the spacecraft due to the vehicle's acceleration against gravity. Additionally, random vibrations radiate upward from the engine along with the vibroacoustics created from aerodynamic turbulence as the vehicle passes

through the transonic portion of its flight [17]. Pyrotechnic shocks can also cause random vibrations of high acceleration and high frequencies as a result of the explosive separation events which occur during boosting [17]. These types of excitations can cause significant problems in the large-area and low-mass structures common in satellites. In many cases, however, the exact launch vehicle for a CubeSat is unknown during the assembly and testing, which creates problems when mission planners look to test their satellites for static or random vibration loads that are specific to different launch vehicles. To account for this issue, NASA has released the GSFC-STD-7000 document, which “provides requirements and guidelines for environmental verification programs for GSFC payloads, subsystems and components and describes methods for implementing those requirements” [5].

In order to estimate the typical loading on a CubeSat when the launch vehicle is unknown, mission planners often compare the loads and vibrations of launch vehicles that have been previously used for CubeSats. Most of these vehicles have well documented information on the longitudinal and lateral g-loading, as well as random and harmonic vibration loading over different frequencies [2]. Table 2 lists the maximum longitudinal and lateral loads for three frequently used launch vehicles, while Figure 7 shows the random vibration profile of multiple, frequently-used launch vehicles. These figures are shown in an *acceleration spectral density* (ASD) versus frequency plot [18, 19]. This type of plot “describes the frequency content of the vibration and is equal to the mean-square acceleration ( $g^2$ ) in the selected frequency band divided by the width, in Hz, of that band. The square root of the area under this curve represents the time history’s

root mean square (RMS) value, which is equivalent to one standard deviation,  $\sigma$ , or the random acceleration” [5].

With this type of information, mission planners are able to find and test for the highest recorded loads and vibrations, based on previous launches. The results from simulated or physical tests under these conditions are then compared with the GSFC-STD-7000’s minimum probability-level requirements for each type of load to investigate how well the CubeSat responds to each type of load, and to determine whether or not it is ready for launch. If the structure or any component within the spacecraft happens to fail any of these tests, developers must choose different structural or internal layouts in order to prepare the vehicle for a survivable mission. Table 2.4-1, Structural and Mechanical Verification Test Requirements, in the GSFC-STD-7000 document explains the nature of all required verification tests on a component level. This includes whether or not actual, physical tests are required in contrast to simulations. According to Cal Poly’s *CubeSat Design Specifications*, these requirements must be met when a Launch Vehicle (LV) provider is unknown.

**Table 2 - Typical Launch Loads of Past CubeSat Launch Vehicles [18]**

<b>Launch Vehicle</b>	<b>Max. Longitudinal G-Loading and Time</b>	<b>Max. Lateral G-Loading and Time</b>
Dnepr	+8.3 g’s at 2 <sup>nd</sup> Stage Burn	0.8 g’s after LV exit from transport launch canister
Eurockot	+8.1 g’s at Stage I Engine Cut-Off	+/-0.9 g’s due to max. dynamic pressure
Minotaur I	+6.6 g’s at 2 <sup>nd</sup> Stage Ignition	+1.6 g’s at Liftoff

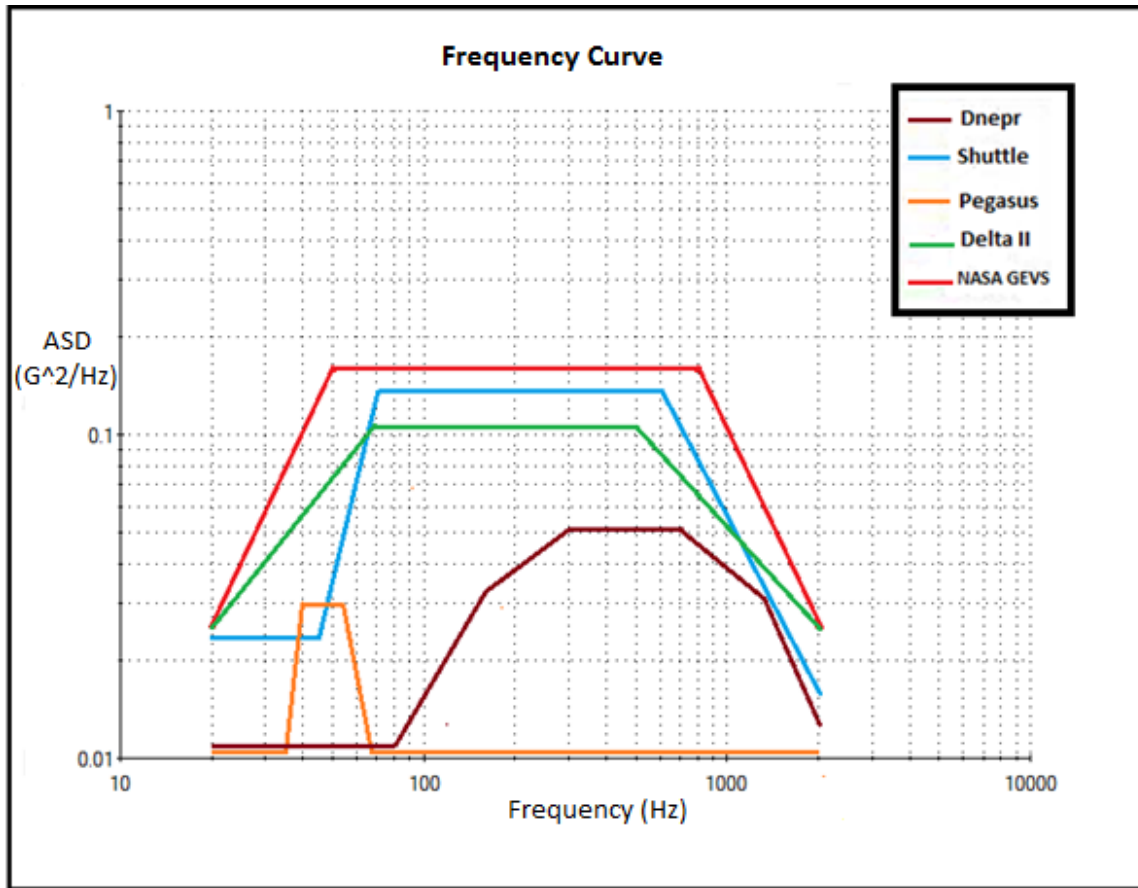


**Figure 7 - Random Vibration Profile for Various CubeSat Launch Vehicles [19]**

To make this process easier, NASA’s GSFC-STD-7000 document defines a “worst case scenario” random vibration profile, shown in Figure 7 by the green line. This profile defines the acceleration spectral density as a function of the frequency during a “worst case scenario” launch, and can be used as a guideline during simulated or physical testing. By performing a random vibration analysis under this specific condition, mission planners can be sure that they have tested for the highest vibrational loads that the CubeSat will likely encounter.



## 2.3 Thermal Subsystem

### 2.3.1 2010-2011 WPI CubeSat MQP Recommendations

The thermal analysis from the 2010-2011 Major Qualifying Project, “Design and Analysis of Subsystems for a CubeSat Mission,” suggests that the greatest concern facing the CubeSat is the loss of thermal energy while the satellite is in eclipse. The team suggested that multi-layer insulation (MLI) should be installed to reduce the amount of heat lost while the satellite was not in sunlight. MLI is a type of thermal blanket used on various satellites because of its low mass, low volume, and simplicity.

MLI is made up of multiple, thin layers of a low conductivity material. The most common type of layer is made out of a 0.25mm thick sheet of Mylar. The sheets are constructed so that there are few points of contact between the layers, which minimizes the conductive heat paths. As the number of layers increase, the heat transfer decreases; the lowest heat transfer is normally achieved at approximately 25 layers [17]. From past missions, the expected emissivity<sup>9</sup> for a multi-layer insulation blanket is between 0.015 and 0.030 [17]. Figure 8 shows the relationship between number of layers of MLI and effective emittance.

---

<sup>9</sup> Emissivity is the relative ability of a surface to emit radiation. Emissivity is also defined as “effective emittance” by Wertz and Larson.

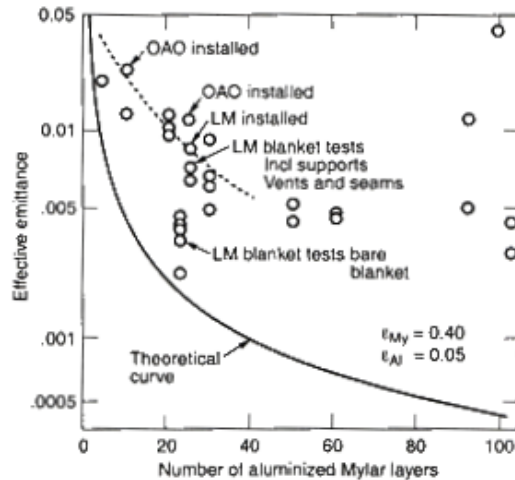


**Figure 8 - Effective Emittance vs. Number of Aluminized Layers for Multi-Layer Insulation [17]**

The 2010-2011 Major Qualifying Project, found that the surface temperature of the satellite during a period of eclipse was 260.8K on the Earth facing side, and 249.1K on the sun facing, solar paneled side. They assumed a surface emissivity of 0.83 the silicon solar cells, and 0.85 for the sides of the satellite with a simulated coating of black paint. The team used 3K for the equivalent blackbody temperature of space, and a flux of  $231 \frac{W}{m^2}$  from the earth.

### 2.3.2 Space Thermal Environment

For a small spacecraft in low Earth orbit, there are three primary sources of thermal radiation that the spacecraft will encounter, which can be seen in Figure 9. Radiation from direct sunlight, which occurs when the spacecraft is not in eclipse, is the largest factor. The fraction of sunlight that is reflected off of the earth, albedo, is also another thermal consideration for spacecraft in Earth orbit. There is also the thermal radiation that the Earth emits at infrared wavelengths that is present regardless of eclipse.

A fourth case, although rare, is that a spacecraft may also encounter free-molecular heating in very low Earth orbits [20].

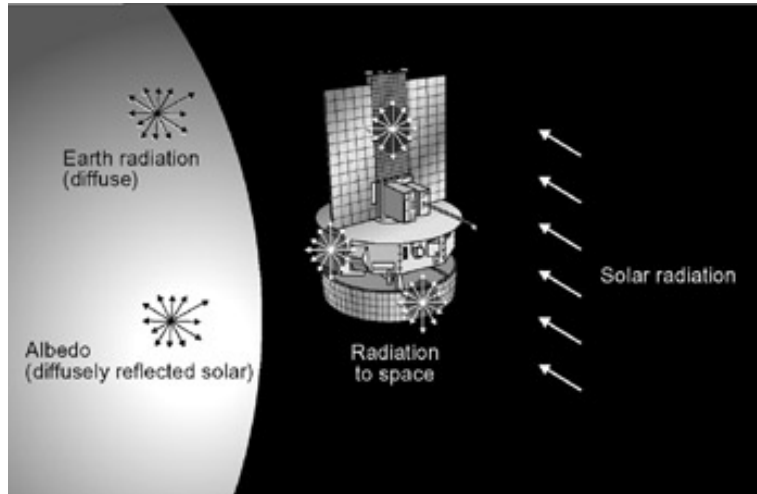


**Figure 9 - Space Thermal Environment [21]**

In space, the thermal energy from the three most intense sources, direct sunlight, albedo, and thermal radiation, can be modeled as radiant heat fluxes [2]. Depending on the time of year, the integrated, radiative flux in low earth orbit from the sun can vary from  $1414 \frac{W}{m^2}$  during the winter solstice and to  $1322 \frac{W}{m^2}$  in the summer solstice. This variation is due to varying distances between the Earth and sun at certain times during the year [22]. The direct solar intensity can be modeled using Equation 2.1:

$$J_s = \frac{P}{4\pi d^2} \quad (2.1)$$

Where  $J_s$  is the total solar intensity,  $P$  is the power output of the sun ( $3.856 \times 10^{26}W$ ), and  $d$  is the distance from the sun in meters [17].

The albedo is the amount of solar radiation that is reflected by the planetary surface expressed as a fraction as seen in Figure 10. Characterized by variable  $a$ , the

albedo can be used in an equation to calculate the total intensity of Earth-reflected radiation:

$$J_a = J_s a F \quad (2.2)$$

$F$  is a visibility factor that is multiplied by  $a$ , which is the planetary albedo fraction, and  $J_s$ , which is the previously calculated solar intensity [17]. The determination of this visibility factor can be seen in Figure 10, where it is a function of altitude and the angle between the spacecraft nadir vector and the sun's rays,  $\beta$  [17].

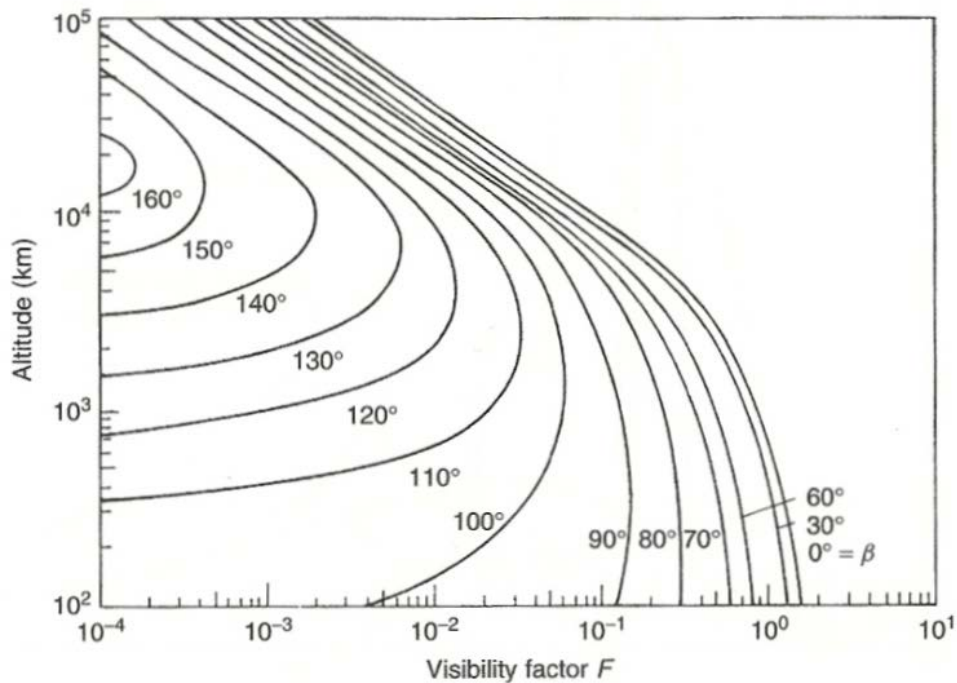


**Figure 10 - Altitude vs. Visibility Factor  $F$  [17]**

However, albedo calculations can become very complex should a large spacecraft have several surfaces elements in different orientations. The albedo value  $a$  will vary depending on the orbital body in question (see Table 3).

**Table 3 - Planetary Albedo Values [23]**

Planet	Solar Radiation Intensity, $J_s$ (Percentage of solar intensity at 1 AU)	Planetary Albedo
Mercury	667	.06 - 0.10
Venus	191	.06 - 0.76
Earth	100	0.31 - 0.39
Moon	100	0.07
Mars	43.1	0.15
Jupiter	3.69	0.41 - 0.52
Saturn	1.1	0.42 - 0.76
Uranus	0.27	0.45 - 0.66
Neptune	0.11	0.35 - 0.62
Pluto	0.064	0.16 - 0.40

The final environmental thermal source for the spacecraft is thermal energy emitted at infrared wavelengths from the body that the spacecraft is orbiting. For Earth, the amount of energy radiated is dependent on the region of the Earth from which sunlight is reflected, as warmer areas emit more radiation more than colder ones. However, since the entirety of the Earth's disc is visible, the variations in thermal radiation from geographical location can be considered negligible [17]. The value of the thermal radiation is:

$$J_p = 237 \left( \frac{R_{rad}}{R_{orbit}} \right)^2 \quad (2.3)$$

Where  $J_p$  is the value of the thermal radiation intensity in  $\frac{W}{m^2}$ , and  $R_{rad}$  and  $R_{orbit}$  are the values of the Earth's radiating surface and orbit radius. It is recommended that the value for  $R_{rad}$  be equal to the radius of the Earth's surface as it can be very difficult to determine. It is important to note that this thermal radiation should not be neglected

because it cannot be deflected with thermal control coatings because of its short wavelength. It is because of this that the blackbody radiation must be considered for spacecraft in LEO. The blackbody temperature for the Earth can be modeled as 218K for the atmosphere, and 288K for the surface.

Another important aspect of the space environment is atmospheric drag in low Earth orbits. Due to the residual atmosphere at relatively low orbital altitudes, spacecraft can experience drag forces. While this may be negligible on small spacecraft, larger ones will often have to boost themselves back up to their design orbit periodically. However, in many cases these forces can be neglected, with atmospheric pressure less than  $10^{-7}$  millibar [17]. While some texts note that this drag force can cause some heat via free-molecular flow a spacecraft would have to be in an abnormally low altitude for this to be a design concern [23].

### **2.3.3 Spacecraft Thermal Control**

Spacecraft are often subjected to environmental extremes as discussed in the previous section, and as such it is imperative to ensure that the thermal characteristics of the spacecraft are understood and regulated. The success or failure of a mission often depends on a spacecraft's ability to stay within two defined ranges of temperature: *the operational temperature range* and the *survival temperature range* [17]. The temperature of surfaces in the spacecraft, relative to these two ranges, are checked by doing a "Worst Case Conditions" analysis in which the temperature extremes the spacecraft could encounter are determined. Usually these extremes correspond to the full illumination of a spacecraft, also known as the "Hot Case," and the full eclipse of the spacecraft, also known as the "Cold Case" [25]. The function of the Thermal Subsystem is to regulate,

either through *active* or *passive* heat transfer methods, the temperatures throughout the spacecraft [26].

The operational temperature range is the range between the maximum and minimum temperature within which the components of a spacecraft are expected to behave normally as reported by the manufacturer. This range can either be listed for a single component or an instrument package, or as is sometimes the case, the range within which all of the combined systems of a spacecraft can operate. For the latter case, the temperature range may potentially be very narrow, as component operational ranges might have very little overlap. A particular mission may need to occasionally exceed operational temperatures for components but as long as they are eventually brought back within range, the component should continue to function as expected.

The survivable temperature range is similar to the operational temperature range, except deviation outside of the range will cause the spacecraft or component in question to potentially malfunction and may even cause the failure of the mission. As stated before, this may either refer to the range of a single component or the spacecraft as a whole.

As it is unfeasible to design a spacecraft or component to exist at a specific temperature, a Worst Case Analysis is often used while examining the thermal profile of a mission. During such an analysis the engineer considers the extremes that might likely be encountered in a mission, and then takes steps to either compensate for these extremes or ensure that the survivable and operational temperature ranges are not exceeded. Often, in a thermal analysis these extremes are divided into a case of full-illumination, which

would cause a maximum temperature, and a full-shadow (or full eclipse), which would cause a minimum temperature.

The first case to consider is the Hot Case, which is when a combination of environmental effects cause the spacecraft to reach the maximum temperature that will be achieved on a mission. This status is determined using a collection of factors including orbital analysis, blackbody radiation, and any resultant radiation from the albedo effect.

The other case encountered is the Cold Case, which is the opposite of the previously mentioned case. As the satellite will continue to receive blackbody radiation from the Earth, the minimum temperature will be found when the thermal effect from direct exposure to the sun and the reflected light from albedo are lowest.

All heat transfer can be modeled as a combination of three key modes; *conduction*, *convection*, and *radiation*. Conduction occurs when energy is directly transferred between two bodies by the molecular interaction of their shared boundary. Conduction heat transfer is present in spacecraft through the direct contact of various structures, systems, and components and plays a large part in the dissipation of heat throughout a spacecraft. Convection occurs as a result of energy being transported from one body to another by means of a participating fluid media. While convection heat transfer could play a role on some spacecraft (e.g. one which uses heat pipes), it is not a factor in determining the total heat flux imparted on the spacecraft by the local space environment. Radiation (more specifically thermal radiation) occurs when energy is transferred due to the excitation of electron configurations of atoms as a result of electromagnetic waves. Radiation is the primary method of heat transfer through which a



spacecraft receives heat from the local environment and also plays a role in controlling the thermal energy balance inside of a spacecraft.

The thermal energy that the spacecraft receives from the environment was discussed in Section 2.3.2, and as such, this section will focus on how a spacecraft may compensate and manage such heat for survival and mission completion.

One option an engineer may consider when completing the thermal design of a spacecraft is a *Passive Heat Transfer* system. These systems are called passive because they operate without any additional power or control in order to maintain a thermal balance. Passive systems are common on a wide range of spacecraft due to their low cost, lack of complexity, and moderate level of effectiveness. A few examples of passive thermal control systems are: heat pipes, radiators, surface coatings, and insulation. These systems allow the engineer to select surface emissivity levels, control conduction paths, and set thermal capacities of insulation systems.

*Active Heat Transfer* is a method in which a system receives power and control, and as a result a heat exchange is produced. While active systems are undeniably more complex than passive systems, they have the advantage of increased capabilities and higher effectiveness. Heat pumps, switches, shutters/louvers, and electric heaters (or coolers) are examples of various active thermal control systems. These systems are typically only used when analysis has shown that passive systems will not keep the spacecraft or components within operational and survival ranges and are most often used for very temperature-sensitive missions with scientific payloads (optics, batteries, and sensors).

## **2.4 Power Subsystem**

### **2.4.1 2010-2011 WPI CubeSat MQP Recommendations**

The previous WPI CubeSat MQP, completed in 2011 [2], provided a foundation for the power subsystem. This team evaluated two different power system options, one for lab testing and another for flight. Since this year's project is intended to eventually launch, the 2011 "Flight Option" recommendations provided our baseline. For the Flight Option, the previous team researched CubeSat hardware providers, ClydeSpace and CubeSat Kit, and recommended ClydeSpace as the power system provider [2]. The 2011 MQP team chose ClydeSpace due to its extensive flight heritage, conformance to CubeSat specifications and the relatively wide selection of compatible components [2]. The company sells all required power system components for the CubeSat, including solar arrays, batteries and power load management systems. The previous team specifically recommended the following ClydeSpace components: the 3U solar arrays, the 10Whr Lithium-Polymer battery and the Electrical Power System (EPS) [2]. The 2011 team chose these components on the basis of their MQP's requirements and instrument specifications. However, their analysis methods and research proved useful to the present project. We used these recommendations as a starting point for this year's analysis.

The 2010-2011 MQP also began development of a Lab Option solar array. They developed a power management and distribution design, intended to regulate power inputted through an umbilical system [2]. This design was used as a baseline for our project's power management and distribution system. The design and the parts purchased were incorporated into this year's Lab Option design.

### 2.4.2 Determining the Acceptable Load

Solar arrays should be designed to meet the power requirements at the end of the satellite's life (EOL). This results in the satellite producing excess power at the beginning of the mission, which has to be accounted for. At the beginning of the mission (BOM) the array has a power per unit area that can be found using Equation 2.4 [17].

$$P_{BOL} = P_o I_d \cos \theta \quad (2.4)$$

Where  $\theta$  is the angle measured between the spacecraft-sun vector and the vector normal to the solar array.  $P_o$  is the ideal solar cell output, which is typically between  $202 \frac{W}{m^2}$  and  $253 \frac{W}{m^2}$ , based on silicon and gallium arsenide solar cells respectively [8].  $I_d$  is the inherent degradation of the solar array. The inherent degradation is a measurement of how the solar arrays lose efficiency through use. The amount of degradation to the solar array of the satellite is determined by Equation 2.5, in which the satellite's life is measured in years [17].

$$L_d = \left(1 - \frac{\text{degradation}}{\text{year}}\right)^{\text{satellite life}} \quad (2.5)$$

From which the end of life performance [17] can be calculated by Equation 2.6.

$$P_{EOL} = P_{BOL} L_d \quad (2.6)$$

The current-voltage characteristic can be described by a curve that is dependent on temperature. The temperature coefficient is defined as the percent degradation of performance with increasing temperature [17]. The temperature coefficient for the solar array is dependent solar cell type, actual operating temperature, and radiation environment [17]. The peak power point of the current-voltage curve depends on the

array's operating temperature; an array often produces the most power coming out of eclipse because the array is at its coldest. The temperature coefficient is used to establish how the peak power point changes based on temperature changes. Figure 11 is an example of a current-voltage curve for a solar array using silicon solar cells. Through the use of thermal analysis the power the solar array will produce at any given time based on the temperature of the solar array is better understood

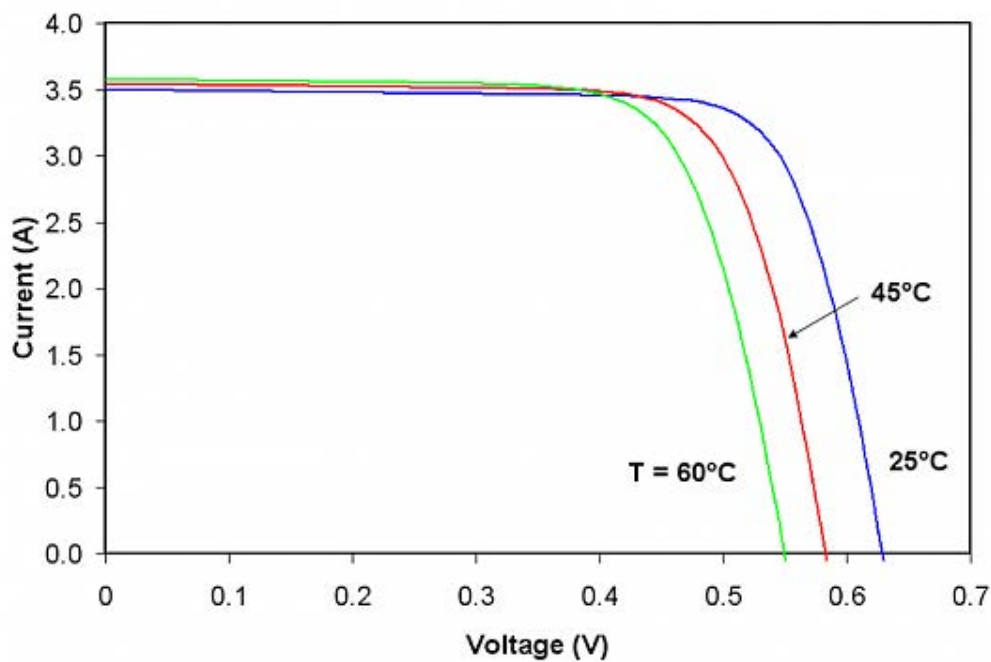


**Figure 11 - Current-Voltage Curve [27]**

### **2.4.3 Power Management and Distribution**

Perhaps the most vital function of the power subsystem is power distribution. Because a CubeSat is extremely limited in its power generation due to its mass, volume and area restrictions, the available power must be budgeted in order to sustain every component. After the team knows how much power the satellite needs, it is imperative that the PMAD system deliver the available power properly. In addition, the PMAD

system must prevent damage to components, manage the battery and provide other power conversion and conditioning. All CubeSats launched in 2010 have included a PMAD system. There are a few commonly used approaches that can fulfill these basic requirements. A direct voltage through the battery and into the components system can be used to power systems directly from the solar panels, though it does not allow for much control and lacks overcurrent protection. As power systems are the most common reason for CubeSat failure, this approach is used only when absolutely necessary [28]. A second option is to custom design a circuit to condition the power and deliver it to each individual component. This approach affords some control and protection over the direct voltage system, but relies upon excellent circuit design and lacks flight heritage due to the unique design. Instead, most flight-ready PMAD systems are vendor-purchased and can reliably handle a wide array of missions since they often have some degree of flight heritage. Another advantage to these is that they are pre-installed with industry-standard R232 and I2C connections such that they can easily connect with components from different vendors [29].

For a flight design exercise not intended to develop a new power system, it makes the most sense to simply use a vendor-purchased PMAD system. Since the primary mission of this CubeSat is to gather data from the Sun rather than testing new technology, many other components will also be vendor-purchased and will use the same connections. In addition, the flight-proven components and the power conditioning capabilities of a vendor's system will increase the entire system's reliability over an unproven, custom design.

#### 2.4.4. Battery Management

The primary purpose of a battery on a spacecraft is to store energy generated by the solar arrays. This stored energy is then discharged to components when power demand is greater than what the solar arrays provide or during eclipse (when the solar arrays provide no energy). The charging and discharging of the battery is regulated, often by a peak power tracking system and/or a shunt regulator [9]. This protects the battery from over-current and under-voltage situations. As explained in *Space Mission Analysis and Design*, a peak power tracking system is a complex set-up that monitors the power system and adjusts the voltage or amperage to avoid an over or under-powered situation. A simpler shunt system diverts excess power into a shunt where it is dissipated [17]. Without this regulation, the battery could be damaged, eliminating the satellite's energy storage capability.

Most satellites incorporate a battery design to store energy, but these designs are based upon the specific mission requirements. Some missions, such as the Delfi-C3, do not even incorporate a battery because the all components are shut down when the satellite is in eclipse [30]. Since the satellite has no power demand in eclipse, only the solar arrays are needed to supply power. However, most satellites do incorporate a battery designed for their mission. These different battery designs range from one battery per cube [31], to four batteries connected in parallel [32]. Most CubeSat designs use Lithium-Ion batteries because they have a relatively high energy density ( $120\text{-}150\frac{\text{Whr}}{\text{kg}}$ ) and can operate for over 5,000 charge and discharge cycles while in LEO [2]. Spacecraft often have more than one of these batteries as an added redundancy in case the primary battery fails.

Engineers have developed different regulation systems for the variety of battery designs available. However, there is no one design that is commonly utilized because designers often build these regulatory systems individually. If designers do not want to build their system from scratch, customizable systems can also be purchased from satellite components manufacturers, such as ClydeSpace. ClydeSpace in particular, sells an EPS that provides battery regulation. This type of system was recommended by the previous CubeSat MQP team [2] and was analyzed as a Flight Option design.

#### **2.4.5 Power Fault Management**

The power fault management system is used to detect, isolate, and correct faults within the power subsystem. The most common type of failure is a short circuit, which draws extra power and may endanger the mission [17]. In order to prevent a mission failure from one short circuit, the electric power subsystem isolates the short through the use of fuses, which can be reset. If required for a particular mission, fault-detection circuits can be used to locate where the fault has occurred.

There are two types of fuses that are generally used on spacecraft, fuse lines and power switches. Fuse lines are connected directly from the power system to the component. These cannot be reset once the fuse is activated, whether the activation is accidental or not. However, the advantage of the fuse lines is that they do not require a dedicated circuit board, and thus take less space than power switches [33]. Power switches are the most versatile method of fault management. These “can be considered as an electronic fuse that automatically switches off when the current drawn by the subsystem becomes larger than a pre-programmed value” [33]. Power switches can be reset after they are activated, just as they would switch power to the subsystem on and

off. Although the fuse lines are simpler, the power switches are better for this CubeSat because they allow for better power control.



### **3. Methodology**

#### **3.1 Research**

Throughout our project, previous CubeSat design reports guided us in developing our analytical tools and choosing components. Our primary reference was the 2010-2011 MQP report, Mechanical, Power and Propulsion Design for a CubeSat [2], which suggested software tools available at WPI and provided recommendations for components. The previous team also compiled an extensive list of CubeSat references, which included other reports about CubeSat development. Our team used these references as additional sources throughout our project.

In addition to utilizing the previous MQP team's work, we found other resources, such as online research and local experts. Since a large portion of our project was component selection, we read specifications and examined CAD drawings available on manufacturer's websites. When the online resources did not provide enough information, we directly contacted representatives at companies such as ClydeSpace and Pumpkin for additional information. We also utilized previous reports and online tutorials to learn analysis software such as SolidWorks and COMSOL. To provide additional assistance with these tools, we also contacted professors and other local experts. These experts also guided us when we had specific research questions. Communication with experts, reports and specifications available online, and the 2010-2011 MQP were the primary resources used during our analysis.

## **3.2 System Engineering Group**

In addition to the mechanical, thermal, and power subsystem groups represented within this report, two additional groups were integral to the overall satellite design. The Mission and Environmental Analysis team was responsible for identifying and monitoring expected conditions for the orbit of the satellite. The Attitude Determination and Control team was responsible for ensuring that both the satellite's orbit and pointing could be maintained. As each subsystem on a satellite is interdependent, it was necessary to coordinate with the other teams throughout the entire design process. To assure this coordination, all three groups met in weekly System Engineering Group (SEG) meetings along with project advisors to discuss any updates or revisions to their respective aspect of the satellite's design. The work of these other two teams is fully documented in the corresponding MQP reports, References [36] and [37].

## **3.3 Mechanical Design and Structural Analysis**

The following section explains the methodology which the mechanical and structural subsystem group used to model and test the Flight Option CubeSat. The section also includes the group's process of designing and building a test fixture which will eventually be used to hold the Lab Option CubeSat in WPI's vacuum chamber for testing.

### **3.3.1 Flight Option Baseline CAD model**

In order to meet the objectives of this project, the mechanical and structural subsystem was tasked with keeping an updated CAD model of the Flight Option CubeSat. This model existed only as a SolidWorks assembly file, unlike the Lab Option CubeSat which was partially manufactured at WPI by the 2010 CubeSat MQP group. The components of the Flight Option were selected and integrated based on recommendations by this year's three CubeSat MQP groups. Throughout the project, the CAD model

served as an organizing, visual aid during SEG meetings, where decisions that affected the internal and external layout of the CubeSat were discussed. The CAD model also provided the mechanical and structural subsystem with a way to test the structural integrity of the CubeSat framework through static and random vibrational loading simulations.

Due to the nature of this continuing MQP, the Mechanical and Structural Subsystem team was immediately given access to the 2010 project's CAD drawings. These models provided a starting point for the 2011 project's CubeSat design, though differences in the two projects' mission requirements called for numerous, large-scale alterations. While the 2010 MQP focused on a Lab Option, our project focused primarily on a Flight Option, which was designed with the intent that it would eventually be launched in the future.

The Mechanical and Structural Subsystem team began organizing the satellite's component layout around a commercially available, 3U CubeSat structure from Pumpkin. This model was chosen due to its well documented flight heritage and the experience of its manufacturer [6]. A simplified drawing of this structure was created by the mechanical and structural subsystem from scratch based on downloadable CAD drawings provided on Pumpkin's website. This simplified drawing avoided any problems associated with mating or meshing of the drawing within SolidWorks since it did not incorporate all of the small features (or require the amount of computer memory) that the downloadable drawings from Pumpkin's website did. From there, CubeSat components were added based on the project's mission requirements and recommendations from each subsystem.

The Flight Option CAD drawing also allowed the mechanical and structural subsystem to simulate static and random vibrational loading on the Pumpkin structural design. This process was done using SolidWorks Simulation, an office product of SolidWorks Professional (provided at no cost to WPI students). Using the Simulation Wizard within the SolidWorks program, the user begins by simply choosing from a list of different tests including static, frequency, buckling, thermal, nonlinear, linear dynamic, etc. After selecting the type of test, the program asks the user to define the model's material, any fixtures applied to the model being tested, external loads, connections, and other parameters based on which type of test is being run. After defining these parameters, the user can run the simulation and obtain results from graphs generated.

For this project, we ran both static and random vibration tests using SolidWorks simulation in order to investigate how the Pumpkin structure responded to typical launch loads. Although producing results for the static load simulation was fairly easy with a basic knowledge of SolidWorks, the random vibration simulation was a little more involved. As mentioned above, the first step involved selecting the "random vibration" test from the "linear dynamic" branch of the test type list. Next, the material was chosen to correspond with that of the Pumpkin 3U structure (Al 5052-H32), and fixtures were applied to the structure in order to simulate the satellite being held inside the P-POD device during launch. A difficult part of this process was defining the external load. To simulate the vibroacoustics of a typical launch condition, we started by choosing the "selected base excitation" option from the dropdown list of external load types. We then selected the "acceleration" option with units of  $\frac{g^2}{Hz}$  and manually input the ASD variation with frequency. Since we wanted to simulate the "worst case scenario" launch, we

entered an ASD vs. frequency curve into SolidWorks based on the General Environmental Verification Standards (GEVS) data from the “Vibroacoustics Qualification” section of NASA’s GSFC-STD-7000 document (see Section 2.2.4) [5]. The simulation was then run using these inputs, and the resulting displacements and von Mises stress were generated. These results were then compared to the material’s yield strength and the GSFC-STD-7000 document’s qualification specifications to confirm that the structure could handle a typical launch without failing.

### **3.3.2 Mechanical and Structural Subsystem Support**

In order to keep the Flight Option CAD model up-to-date, the Mechanical and Structural Subsystem group maintained frequent communication with other subsystem teams. In many cases, things such as power requirements or component locations called for multiple, large-scale changes in the CubeSat’s layout each week. For each new layout, a CAD drawing was created and brought to that week’s subsystem and SEG meetings where it was discussed. These 3D images gave group members and advisors something to visually refer to when describing potential changes or additions to the CubeSat, and ensured that each design complied with Cal Poly’s specifications for size and mass. In some instances, for example with respect to the number of necessary solar arrays and the magnetometer boom mechanism, changes to the CubeSat were decided upon only to be subsequently changed back to the original design. To account for the constant changes, it was the mechanical and structural subsystem’s responsibility to keep an organized folder of the SolidWorks part and assembly files by revision and date. This organization allowed the Mechanical and Structural Subsystem team to easily add or remove components from the updated assembly drawing to make quick changes to the model. If that change ended up being retracted, it was easy to go back and replace the drawing with

its previous model. Also, when necessary, component drawings could be sent out to other subsystems or to our partners at the Space Research Center, Polish Academy of Sciences.

### **3.3.3 Vacuum Chamber Structural Testing**

In addition to the Flight Option, we also made progress with the Lab Option CubeSat which had been partially constructed by the 2010 CubeSat MQP group. As the mechanical and structural subsystem, our main objective for the Lab Option CubeSat was to design and build a test fixture that would hold the CubeSat while being tested in WPI's vacuum chamber. In order to do this, we began by taking measurements of WPI's vacuum chamber, which is located in the basement floor of Higgins Laboratories. After getting the necessary dimensions for the vacuum chamber, we began drafting preliminary designs for the test fixture. These designs were brought to team meetings where simplifications and alterations were suggested to make the fixture affordable and buildable before the project's deadline. Initial designs featured extensive structural support and complex mechanisms for functionality. After two or three drafts, we decided on a simplified test fixture which allowed us to affordably purchase and assemble the parts of the test fixture at WPI. For convenience, we decided to make the structural portion of the test fixture completely from T-slotted extruded aluminum since it easily mated with the T-slotted mounting rails inside the vacuum chamber. The finalized design is shown in Figure 12, which features an adjustable arm that can be used for different sized CubeSats. All materials including a 10-foot long T-slotted aluminum section, seven brackets, and all necessary fasteners were ordered from McMaster Carr. The process of cutting the 10 ft. T-slotted aluminum into the required sections was done using a chop saw located in WPI's Washburn Laboratories.

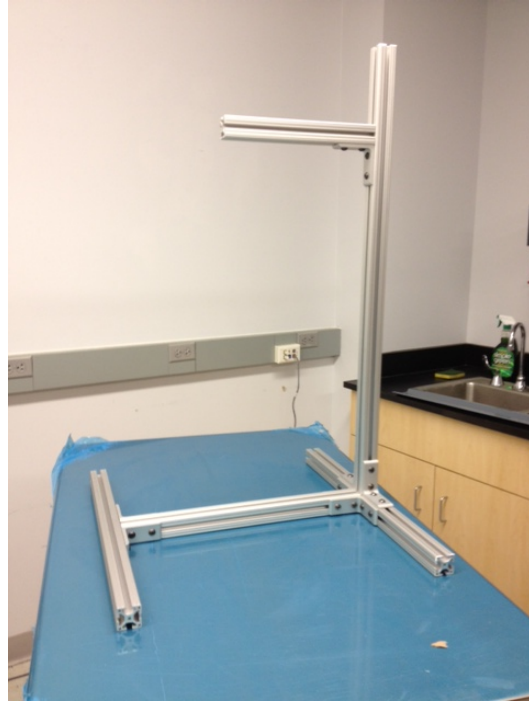


**Figure 12 - Vacuum Chamber Test Fixture Structure**

To accurately test the CubeSat while minimizing external forces such as friction, the plan was to suspend the CubeSat between a top and bottom rail using monofilament line. This design allows only a single degree of freedom, rotationally about the Y-axis (long axis), of the CubeSat. In order to do this, the Mechanical and Structural Subsystem group designed removable caps to secure one end of the monofilament lining to each end of the CubeSat. The other ends of monofilament line would then be secured to the top and bottom center rails of the test fixture and would tighten to suspend the CubeSat in the center of the test fixture. As stated above, this would give the CubeSat the ability to rotate about the long axis of the structure with only the torsional restoring force of the monofilament lining as external resistance. A dimensioned drawing of the CubeSat caps is shown below, with all dimensions shown in centimeters.

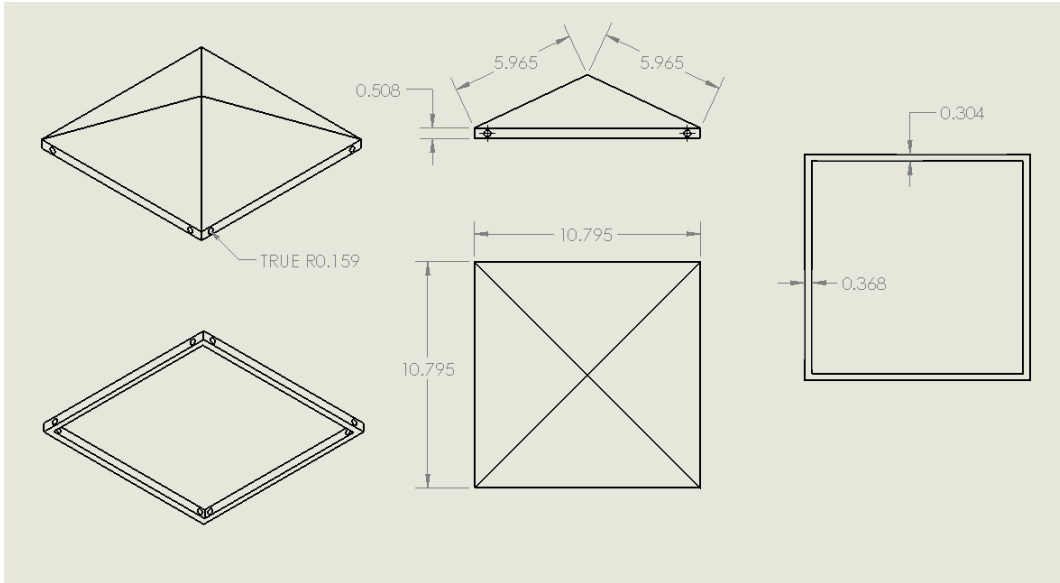


**Figure 13 - Dimensioned Drawing of Caps**

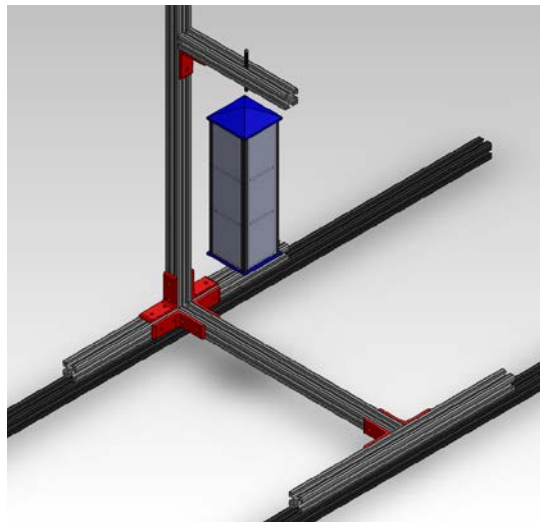


**Figure 14 - Vacuum Chamber Test Fixture with CubeSat and Fine Adjustment Device**

Though not completed by this year’s MQP group, the plan for this test fixture also featured a “fine adjustment” device, which would allow the users to adjust the tension in the monofilament line once the height of the top rail was set. One option for this fine adjustment device is to use two threaded rods which can secure the ends of the monofilament line opposite the caps and be mounted in the top and bottom rails of the



test fixture. Once the threaded rods are set in pre-drilled holes in the top and bottom rails of the test fixture and secured using lock nuts, the rods could be turned to finely adjust the tension in the monofilament lining (which is attached to both the rods and the caps on the CubeSat). Due to time constraints of the project, we were not able to build this fine adjustment device into the structure of the test fixture. A drawing of what the finished CubeSat test fixture will look like is shown in Figure 14 (without the monofilament line or the threaded rod in the bottom rail included in the drawing). This test fixture serves as one potential option for future WPI CubeSat teams to explore.

### **3.4 Thermal Analysis**

The goal for the thermal analysis was to model the expected CubeSat temperature distribution in orbit. In order to do this, we sought to model the temperature distribution to help us come up with recommendations to keep components of the satellite within their required temperature ranges. Additionally, we planned to make any other thermal recommendations that became apparent throughout this process. Our approach to the thermal modeling of the satellite was to split the modeling tasks into separate models of external and internal components, and then to combine the two models once we were confident in each.

#### **3.4.1 Modeling of External Components**

Our group decided to use COMSOL to perform a thermal analysis of the CubeSat model. COMSOL is a finite element method solver that can simultaneously integrate multiple physics modes (e.g. structural and thermal analysis). COMSOL was chosen due to its ability to import SolidWorks models and for its extensive thermal modeling capabilities. Another option considered, but not used, was the thermal modeling tool

within SolidWorks. The 2011 CubeSat MQP cautioned that while it was easy to share models with other design teams, it was not as powerful as COMSOL.

Our first task was to understand how COMSOL imported SolidWorks models. This was important because the Mechanical and Structural Subsystem group was using SolidWorks to create their drawings. COMSOL could import SolidWorks models easily, albeit with some caveats. Our group ran into issues importing models that had been made using specialized techniques or assemblies saved as “welds,” which is a SolidWorks feature that specifies the way components are mated. In cases like these, COMSOL was able to import the model, but not able to mesh it without errors. Due to this, many of the components downloaded from suppliers’ websites could not be directly imported into COMSOL, and instead had to be recreated. Because of the CPU-intensive nature of meshing, many geometries were simplified or altered in order to avoid long mesh times. Figure 15 shows an example of a refined mesh for our model, in which large flat areas like the solar panels could use coarser mesh elements, where more complicated areas needed extremely fine mesh elements.

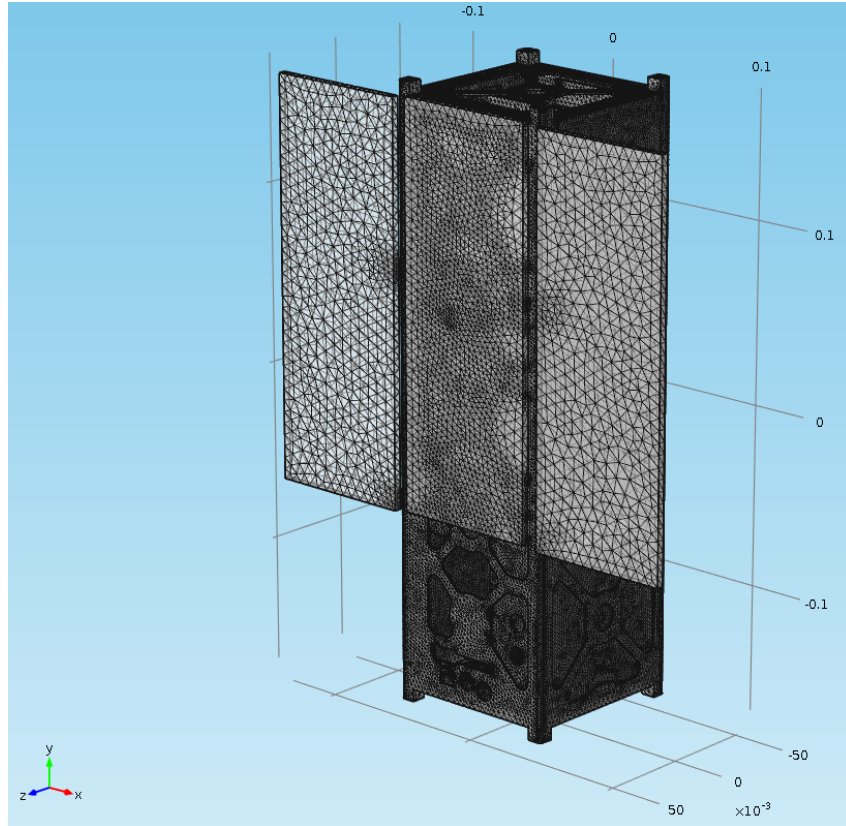


**Figure 15 - COMSOL Mesh of the CubeSat**

To assume the heat generated from sunlight, we used COMSOL’s built-in physics package for a general inward heat flux. There were three options to choose from for the heat flux, which were “General inward heat flux”, which added a value in  $\frac{W}{m^2}$  to the total heat flux the solver would normally compute across the selected boundary. “Inward heat flux” and “Total heat flux” were other two options, which were designed for heat fluxes that depended on the geometry shape. For this reason we chose to use the “General Inward heat flux” boundary condition. For the purposes of model simplification, the heat fluxes were only applied to flat surfaces of the spacecraft, which were the solar panels and flat aluminum faces.

Another set of boundary conditions we used in COMSOL were the thermally resistive and conductive layers. It was brought to our attention that the default boundary interfaces COMSOL uses between assemblies might not adequately represent real life interfaces. In order to assume adequate contact between different assemblies, the thermally resistive layer was used. This was done primarily by experimentation on simpler geometries to visualize the effect that it would have on the final CubeSat model, and to verify that they would have the desired effect.

Figure 16 shows our implementation of thermally resistive and conductive physics nodes in tandem on a simple geometry. In this case, the thermally conductive layer is used between the thin square plate and the thicker square box. As expected, the steady-state temperature between the two geometries is nearly identical, proving that the thermally conductive layer allows for adequate heat transfer. Between the cube and the cone at the top of the assembly was a thermally resistive layer.

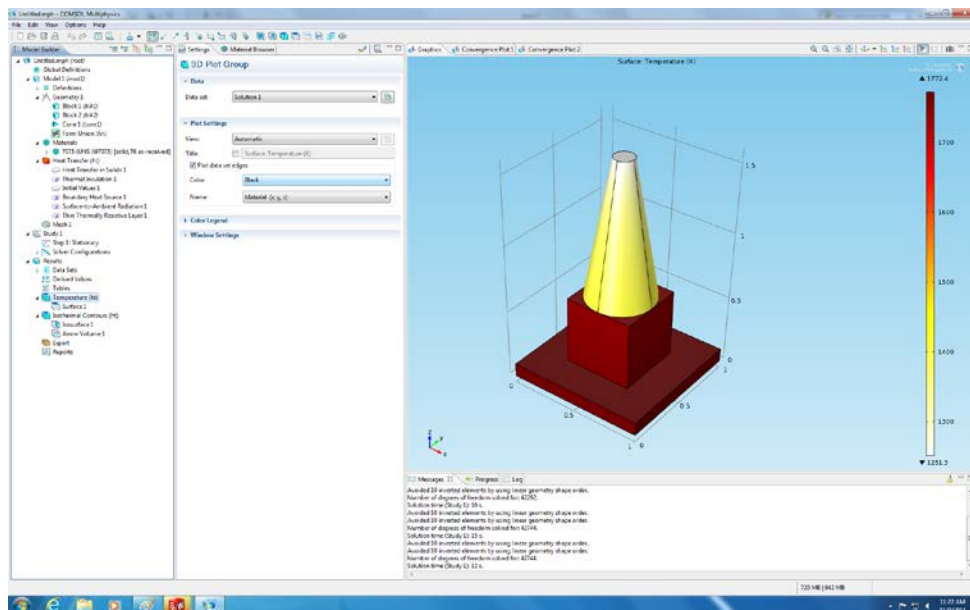


Figure 16 - Tests with Thermally Resistive and Conductive Layers

The knowledge of the thermally conductive and resistive layers was applied to points of interest on the CubeSat model, namely the hinges between the solar panels and the CubeSat body. The equation for a highly conductive layer found in COMSOL is as follows:

$$-n \cdot q = d_s(Q - \rho_s C_s \frac{\partial T}{\partial t}) - \nabla_t \cdot (-d_s k_s \nabla_t T) \quad (3.1)$$

The variable  $q$  defines the net outward heat flux through each face of the layer, where  $n$  defines the unit normal vector. The layer thickness  $d_s$  is used to describe the layer between the two surfaces.  $C_s$ , the layer heat capacity,  $\rho_s$ , the layer density, and  $k_s$ , the layer thermal conductivity, are all defined with COMSOL's built-in materials database.  $T$  is the temperature, calculated by the iterative solver. In our analysis, we typically used default values provided by COMSOL. It was within our best interest to assume the layer thickness was small enough to be realistic with our model, and every other value was filled in by the solver itself.

While designing our model, we realized that, in order to accurately model radiation to space, we needed to find a boundary condition that would allow selected boundaries to radiate to space modeled as a blackbody. In order to simulate radiation to space, the Surface-to-Ambient module of COMSOL was used. It is defined by the equation:

$$q = \varepsilon \sigma (T_{amb}^4 - T^4) \quad (3.2)$$

Where  $q$  is the total inward heat flux,  $\varepsilon$  is the surface emissivity, and  $\sigma$  is the Stefan-Boltzmann constant, which is predefined as  $5.67 \times 10^{-8} \text{ J s}^{-1} \text{ m}^{-2} \text{ K}^{-4}$ .  $T_{amb}^4$  is the

fourth power of the ambient temperature, and  $T^4$  is the fourth power of the body's temperature. Though an iterative process, COMSOL is able to determine how much heat is radiated in the form of an internal heat flux over time.

The only parameters that must be defined are the surface emissivity and the ambient temperature. We found that surface emissivities are purely a function of the finish on a material, which is useful for thermal control. An emissivity of 1 signifies that the body is a perfect blackbody, while an emissivity of 0 indicates that the body will emit radiation at a fraction of its perfect black body state. The surface-to-ambient radiation was computed by simplifying the spacecraft into three main materials: aluminum for the body, silicone for the solar panel substrate, and copper for electronic components. We defined each material's emissivity individually, as COMSOL's built in model library did not have default values.

Through our literature review, we determined that aluminum can have vastly different emissivities, as a result of the coating choice or finishing choice of the aluminum. For the purposes of our model, we started with the value for simple anodized aluminum, which has an emissivity of 0.77 [35]. With this as a baseline, the value can be changed depending on the needs of the thermal control engineer.

The emissivity assumed for copper was 0.83, which was found through our literature review and raised by a small factor because of its assumed use as a conductor [35]. This value can be changed based on the electronic components being used in the spacecraft. The solar panel substrate was assumed to be silicon, based on the information from ClydeSpace, with an emissivity of 0.85, assumed to be controlled by ClydeSpace.

Our group's next task was to experiment with and learn how to use COMSOL's physics packages, such as the Heat Transfer module. This was accomplished by using COMSOL's Heat Transfer in Solids module on increasingly more complicated CubeSat models. We chose to use the "Heat Transfer with Radiation" option because it provided us with the ability to choose physics that allowed any surface of our satellite to radiate to a vacuum. Within the Heat Transfer with Radiation option, we could specifically radiate energy to space by using a boundary condition called "Surface-to-Ambient" radiation, in which we defined boundaries that would radiate heat. As we became more comfortable with COMSOL, we advanced to more detailed CubeSat skeletons and began to use materials that we could encounter on the Flight Option CubeSat.

In order to model the entire satellite accurately, we needed to import SolidWorks assemblies into COMSOL. Our literature review indicated that the satellite temperature depended heavily on the interface between the solar panels, hinges, and chassis. In order to alter boundary interfaces in assemblies, we used two boundary conditions, "Highly Conductive Layer" and "Thin Thermally Resistive Layer" to model the interface boundary conditions. An example of the selection of these faces is seen in Figure 17. We made extensive use of the Highly Conductive Layer to ensure that the solar panels behaved as if they were a part of one contiguous structure. This allowed us to assume a case where most of the heat was transmitted out of the solar panels and in to the CubeSat structure.

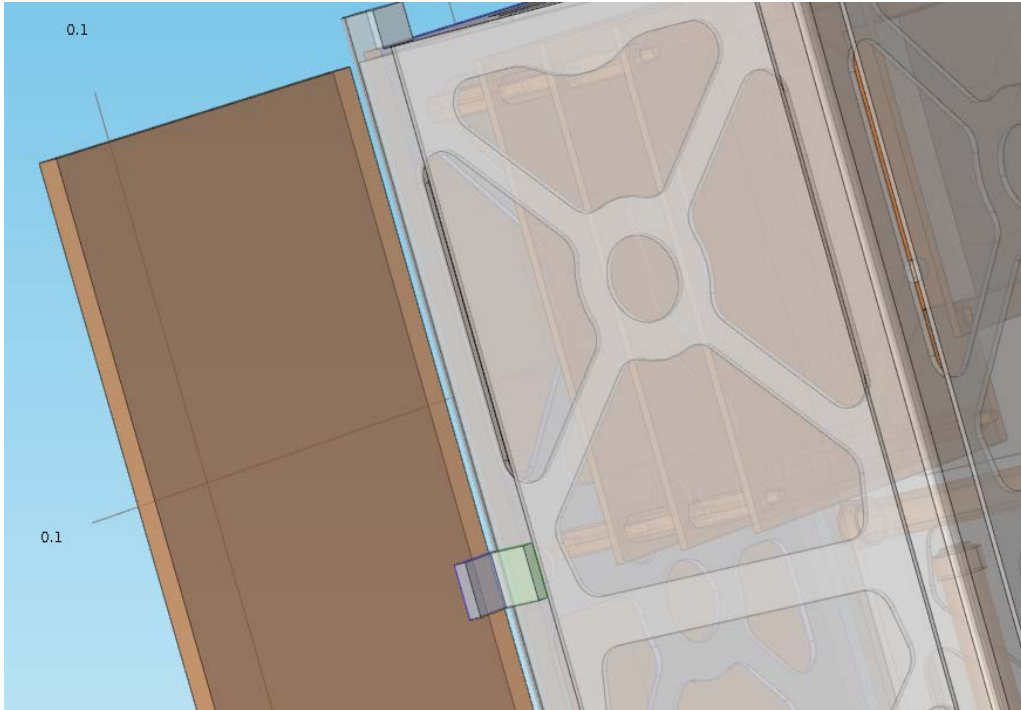


**Figure 17 - Selecting the Boundaries for Highly Conductive Layers**

We ensured that our COMSOL model made use of COMSOL's built in materials library in order to more correctly model heat transfer. Based on the CubeSat specifications, models were initially run with the structure made of Aluminum 6069. However, Pumpkin, the company that manufactures the CubeSat skeleton, uses aluminum 7071. Once our group had decided to use the Pumpkin structure, the models were changed to the correct material.

After the completion of a basic COMSOL model, the next step in our satellite analysis was to determine if there were any trends over multiple orbits. Previously, all satellite thermal simulations were done with a stationary model, in which the analysis is performed until a steady state solution is reached. This had not allowed us to view what happened over any given time, so instead we chose to use a time-dependent model. This



allowed us to specify a time range to compute solutions, and also to specify a solution time step. Varying the solar flux over time in COMSOL involved setting up a varying analytic function. This was accomplished by specifying a rectangular function in COMSOL, which represented one period. The rectangular function was defined as:

$$rect(t) = \begin{cases} 0 & \text{if } t < 360 \\ 1 & \text{if } 360 > t > 3136.8 \end{cases} \quad (3.3)$$

COMSOL called for the rectangular function to have a defined upper limit. We defined the upper limit as one-half of the 400km orbit period (5553.6 seconds) shifted 360 seconds, which came to 3136.8 seconds. The amplitude of the rectangular function varied from 0 to 1. The rectangular function had “smoothing” applied to reduce solver errors and to approximate a transitional period in which the satellite is partially obscured by the Earth. We found that sudden shifts in the function may have caused errors. The rectangular function in COMSOL allows the user to define an area as a transition zone, in which the function will gradually increase to 1. To solve this, we defined the transition as 360 seconds, as it was the lowest value which did not return an error. The function was shifted forward 360 seconds in response to the function’s starting to transition before 0 seconds. The smoothing effect can be seen in Figure 18, where the function gradually increases and decreases between two values as opposed to abrupt transitions.

Next, an analytic function was defined to periodically repeat the rectangular function over time. This was accomplished by using the expression:

$$(mod(t[1/s], p1\_400)) \quad (3.4)$$

Where p1\_400 was a parameter defining the period time of the 400km orbit. The modulus function repeated the orbit, with the plot parameters allowing the function to repeat out to 10 times the orbit. The resulting output is shown below in Figure 18.

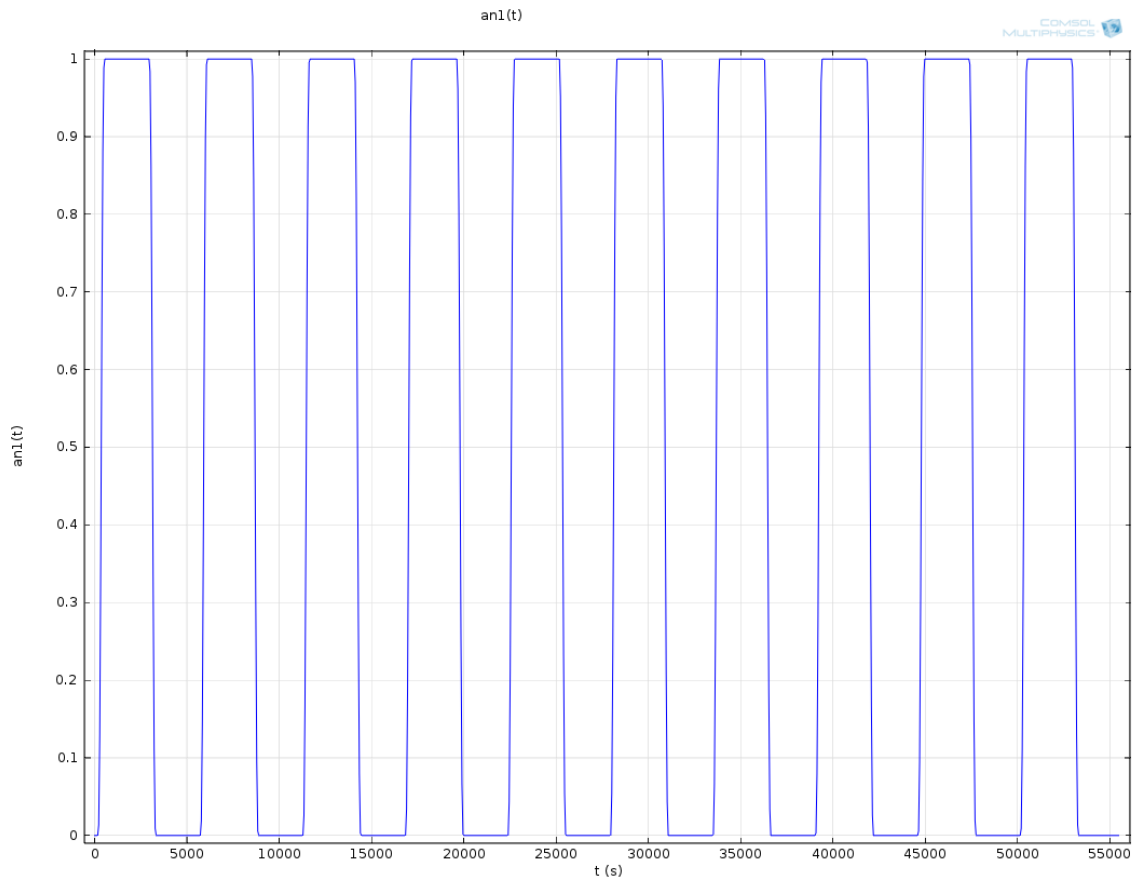


**Figure 18 - Analytic Function to Vary the Solar Flux over 10 Orbits**

With the periodic function defined, the next step was to incorporate it into the physics module. We entered the heat flux as a function of the thermal constant multiplied by the analytic function varying over time. We used two separate sub-modules in order to model both the front and the rear of the satellite over the entire orbit. The equation used for the front of the satellite was:

$$earthflux + (an1(t) \cdot sunflux) \quad (3.5)$$

Where *earthflux* was the heat flux of the earth blackbody ( $245 \frac{W}{m^2}$ ), and *sunflux* was defined in COMSOL's parameters as the solar flux constant minus the earth flux constant ( $1121 \frac{W}{m^2}$ ). The function *anI(t)* called the varying periodic function with respect to time *t*. When the function returned 0, meant that the satellite was in eclipse and the only heat flux it could be receiving was from the *earthflux*, or  $245 \frac{W}{m^2}$ . When the *anI(t)* function returned 1, it meant that the satellite was in direct sunlight and receiving  $1366 \frac{W}{m^2}$ , the maximum value that can be received. We defined the heat flux on rear of the satellite in a similar manner:

$$(anI(t) \cdot earthflux) \tag{3.6}$$

When *anI(t)* returned 1, the satellite was in a position between the earth and the sun so that the rear of the satellite was receiving a heat flux from the earth blackbody. When the function returned 0 and the satellite was in eclipse, the rear of the satellite would no longer receive any heat flux.

After the framework for the external time varying heat flux conditions was set up, the next goal in the thermal analysis was to integrate the internal components of the satellite. One of the main goals of our thermal analysis was to be able to support recommendations to modify the structure or placement of components based on the predicted thermal results. A large part of this analysis was dependent on the operational and survivable temperature ranges of many components throughout the satellite.

Several internal components were modeled separately from the external model. Due to the complexity of the external mesh, internal components were created and

meshed independently and tested in COMSOL for mesh errors before they were integrated into the external model. Once each internal component was verified in COMSOL for consistency, we could add it to the SolidWorks model of the final satellite and reimport it into COMSOL. The following section describes the details of how we modeled and added these internal components to the final model.

### **3.4.2 Modeling of Internal Components**

During a mission, the spacecraft's internal components affect the overall temperature profile through conduction and radiation. The internal components transmit heat through radiation and conduction. However, the radiation flux produced by the internal components is much less than that produced by the Sun or the Earth. For this reason the internal component radiation is neglected as a source of heat. The primary source of heat transfer for the internal components is assumed to be conduction.

A thermal model of each internal component was created in COMSOL in order to evaluate the thermal properties of the spacecraft. We used COMSOL because the rest of the thermal analysis was already being done in the same software suite. COMSOL also has a large number of predefined physics models for different applications. One of these predefined physics models is radiative heat transfer from surface to surface.

Each of the COMSOL models for the internal components had to simulate the materials and the level of power dissipated as heat. Most of the information about the internal components for this project was not readily available from the manufacturers. This made creating an accurate model difficult and required some engineering judgment with respect to the model. COMSOL has difficulty modeling complex systems, and takes

a long time to run any realistic simulation. Since each internal component was to be included in a final model which incorporated all of the components and effects from the earth and sun, it was important to make the models as simple as possible without sacrificing accuracy. The simplification was done by having the solid models in SolidWorks retain only the most important features, and the thermal model in COMSOL assumed all heat released by a given component could be modeled as a singular heat source.

Once the model for the flight option CubeSat was created, we set the framework for a Lab Option CubeSat thermal analysis. Our team set out to verify our COMSOL model with an experiment in the large vacuum chamber. The goal of this approach was to ensure that the temperature results from a COMSOL simulation would be comparable to results found from the Lab Option model.

### **3.4.3 Laboratory verification of COMSOL model**

This subsection outlines our plan for the verification of our COMSOL model using an experiment in a vacuum chamber. We planned to place an aluminum CubeSat model into the large vacuum chamber in the basement (HL016) of Higgins Laboratory on a test stand designed by the Mechanical and Structural Subsystem team. A cryopump on one side of the vacuum chamber (see the left side of Figure 20) would be used to pump the chamber down below 50 milliTorr and would also provide the model with a view towards a cold surface, simulating the cold of space. On the opposite side, a halogen lamp would simulate the radiant heat flux from the sun.



**Figure 19 - CubeSat Model for Lab Option**

Last year's CubeSat model, shown in Figure 19, was used in the vacuum chamber, due to its similarity with our planned geometry and material, and the relative ease with which it could be modeled in COMSOL. A simple COMSOL model was a necessity in order to ensure that mesh errors or complicated geometries would not add additional variables or errors to the output.

Due to the expense of a true sun-simulating heat lamp, we chose simple halogen lamps to simulate heat flux. It was important to note that these lamps would have to function in a vacuum. In addition, to ensure that the Lab Option matched the COMSOL model, we have to determine the theoretical radiative output of the lamps.

In order to get accurate temperature data from the aluminum structure, the plan was to place five thermocouples at various spots in order to measure temperature. These

thermocouples would be placed at the structure's intersections, facing the cryopump, and facing the heat lamp. We then created A LabView Virtual Instrument to read the data from the thermocouples and output it in a temperature vs. time plot.

The temperature data collected from the tests in the vacuum chamber could be compared to the COMSOL model by using the point select tool. In the COMSOL results window, new plots can be created that allow the temperature at a given point on the structure to be displayed as a function of time. The COMSOL model would be created as a time-dependent solution, with the total time being the same as the time set in the lab experiment.



**Figure 20 - Vacuum Chamber to be used for Testing the Lab Option**

Results from the Lab Option test were designed to help verify the Flight Option COMSOL model. If results from the Lab Option COMSOL model show a significant

discrepancy with those found in the vacuum chamber tests, additional research will be required in order to investigate any discrepancies that are found.

## **3.5 Power Analysis**

### **3.5.1 Power Budget**

One of the primary objectives of the power subsystem team was maintaining a detailed power budget (listing supply and demand for different operational modes during the mission). The power from the solar cells changed as the structure of the CubeSat evolved. For example, in the design where the magnetometer used an additional solar array as a boom, the power supply increased. We constantly updated the calculated BOL (Beginning of Life) power supply using the equations explained in Section 2.4.2 of this report. This process was simplified because we were able to use a MATLAB code developed by Andrew Bigelow (member of 2010-2011 Design of a CubeSat [2]) to quickly calculate the BOL power. This code took sunlight vectors from an STK orbit and multiplied them by the solar constant to get sunlight vectors over a particular orbit. The assumptions made in the code to calculate BOL power were full illumination ( $\Theta = 90^\circ$ ), and no inherent degradation. ClydeSpace guarantees a minimum efficiency of 28.3 %, which accounts for degradation. The other required values for solar array area and efficiency were given by ClydeSpace. We verified our results by comparing them to ClydeSpace's results.



**Table 4 - Component Power Demands**

Component	Part Number	Peak Power (W)	Nominal Power (W)	Quiescent Power (W)	Current (mA)	Voltage (V)
GPS	SGR-05U	.080	0.080	.080	16	5
OBC	Pumpkin	0.300	0.300	0.000	TBD	TBD
Magnetorquers (3)	Zarm Technik AG MTO 2.1 (Optimized)	0.420	0.420	0.420	28	5
Sun Sensor	ComTech AeroAstro	0.050	0.050	0.050	3.5	N/A
Gyro	ADXRS450	0.030	0.030	0.030	6	Variable
Magnetometer	Honeywell HMC5883L	0.001	0.001	0.000	0.25	3.6 (max)
Instrument		8.000	8.000	1.000	TBD	TBD
EPS Board	ClydeSpace	0.1	< 0.1	< 0.1	TBD	TBD
PDM Board	ClydeSpace	0.160	0.160	0.160	TBD	TBD
PPM	ARM922T	0.180	0.180	0.180	TBD	TBD
UHF Transceiver		2.000	2.000	0.000	TBD	TBD
<b>Total</b>		<b>11.321</b>	<b>11.321</b>	<b>2.020</b>		
<b>Total Available</b>		<b>12.520</b>	<b>12.520</b>	<b>12.520</b>		
<b>Margin</b>		<b>1.199</b>	<b>1.199</b>	<b>10.500</b>		

During the course of our project, we also tallied the power demands of components chosen by the other subsystem groups. The power requirements of each component were then tabulated as shown in Table 4. Values that labeled TBD were not published. Peak power is the most power that the device will require during operation. Nominal values reflect the power at which the device typically operates. Quiescent power is how much power the device uses while off or in “sleep mode.” The totals at the bottom sum the peak, nominal and quiescent power requirements. Once the total values were determined, they were compared to the calculated  $P_{EOL}$  to verify that the number of solar cells would be sufficient.

### 3.5.2 Baseline System Analysis

In order to adhere to a power budget, it was necessary to determine how both power and data (necessary to control power through a feedback loop) would flow

throughout the system. By developing a baseline component setup of the system, it would become clear how each component interacts and where they fit with regard to power distribution. To this end, the team developed a diagram to visualize where power would need to be directed, as well as the required and available voltages. This allowed us to trace the required power path for each component and ensure each component receives the appropriate voltage. Furthermore, such a diagram can also serve as a preliminary wiring diagram as it indicates which components need to be directly connected.

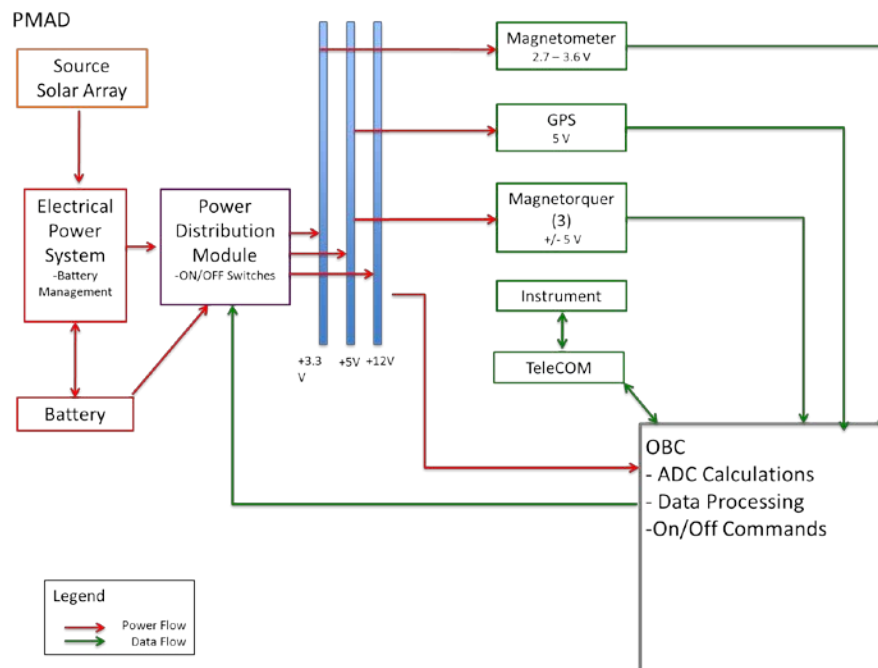


**Figure 21 - Power Management and Distribution Architecture Block Diagram<sup>10</sup>**

As seen in Figure 21, power is generated by the solar array and routed through an EPS. The EPS then delivers this power either to the battery to be stored or to the PDM, where it will be it will be controlled and distributed along three buses: +3.3 volts, +5 volts, or the raw battery voltage (shown here as +12 volts, but is actually equal to the

<sup>10</sup> For the sake of space, this diagram uses the following acronyms: “OBC” stands for On-Board Computer. “ADC” stands for Attitude Determination and Control. “GPS” stands for Global Positioning System.

unaltered voltage provided by the battery). In addition to dividing the power along three buses, the PDM also features on/off switches to regulate power for individual components. From the PDM, each component is connected to one of the three buses, whichever is closest to its required voltage. As the PDM is only able to condition power by turning a switch on or off, each component that operates within a range of voltages will need to perform some fine conditioning itself.

In addition to power flow, Figure 21 also outlines data flow to describe the process for controlling power throughout the system. As seen above, signals pass from the various sensors to the On-Board Computer (OBC). The OBC then performs the necessary calculations to determine how much power each component needs at a given time and gives commands to the PDM. The OBC is also responsible for processing any other data from the instrument.

### **3.5.3 Lab Option Solar Cell Baseline Testing**

In order to verify our proposed power system, it was necessary to determine if our solar arrays were capable of producing the required power during flight. To accomplish this, the team applied a multi-tiered approach, beginning with theoretical calculations as discussed in Section 2.4. Since the theoretical calculations looked promising, the team moved forward with practical Lab Option tests using solar cells from Hobby Engineering purchased by the previous MQP group.

The team began by verifying the solar cells were functioning properly and had not been damaged since the 2010 MQP. As seen in Figure 22, the team connected a single solar array (drawn as a source) in parallel with a voltmeter and in series with both an ammeter and a resistor (to simulate a load). Our test setup placed the solar cell in full

illumination approximately 22.75 inches below a one million candle-power halogen light. This allowed us to determine if the solar cells were producing approximately the same voltages and verify that they were delivering a current.

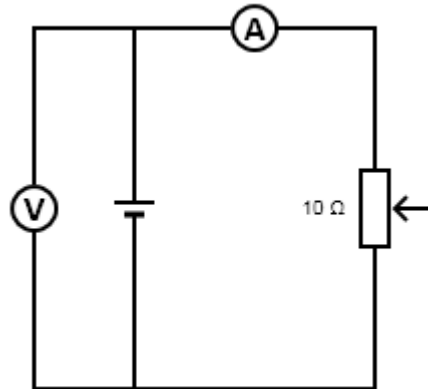


**Figure 22 - Solar Cell Test Circuit Diagram**

After verifying that all eight solar cells were working, the team needed to determine the maximum power point for the solar cells in order to determine the amperage and voltage at which the solar cells operate at their maximum capacity. By changing the resistance used to test the solar cell, it is possible to generate different values for both voltage and amperage. Plotting these points allows us to see where the product of both is as large as possible (i.e. generating the most power). This plot is known as an I-V curve (see Figure 24 for an example). The team connected a solar cell using the same setup as for our functionality testing, using a potentiometer instead of a resistor. This simple change would allow us to test the solar cell at several different resistances without needing to exchange components, thereby reducing error. Figure 23 shows this test in progress. This test would allow us to construct the I-V curve in Figure 24 that suggested a maximum power point at approximately 2.29mA and 5.67V.

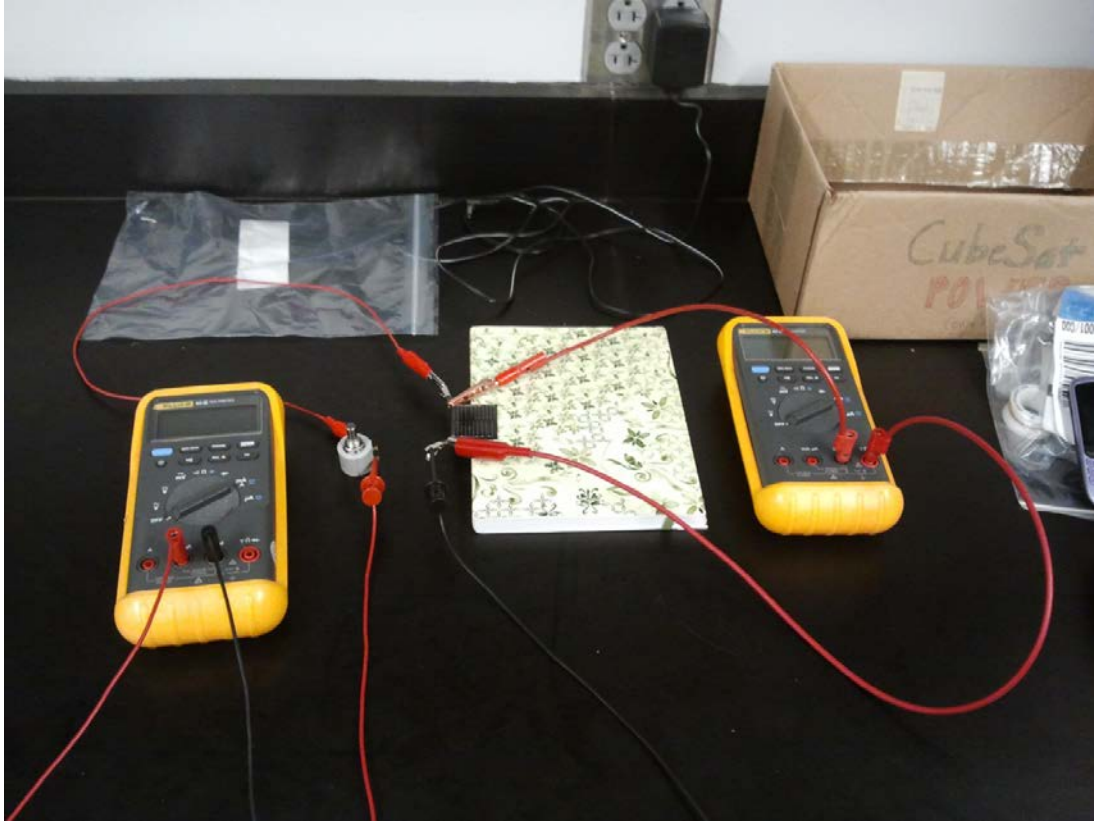


**Figure 23 - Solar Cell Testing In Progress**

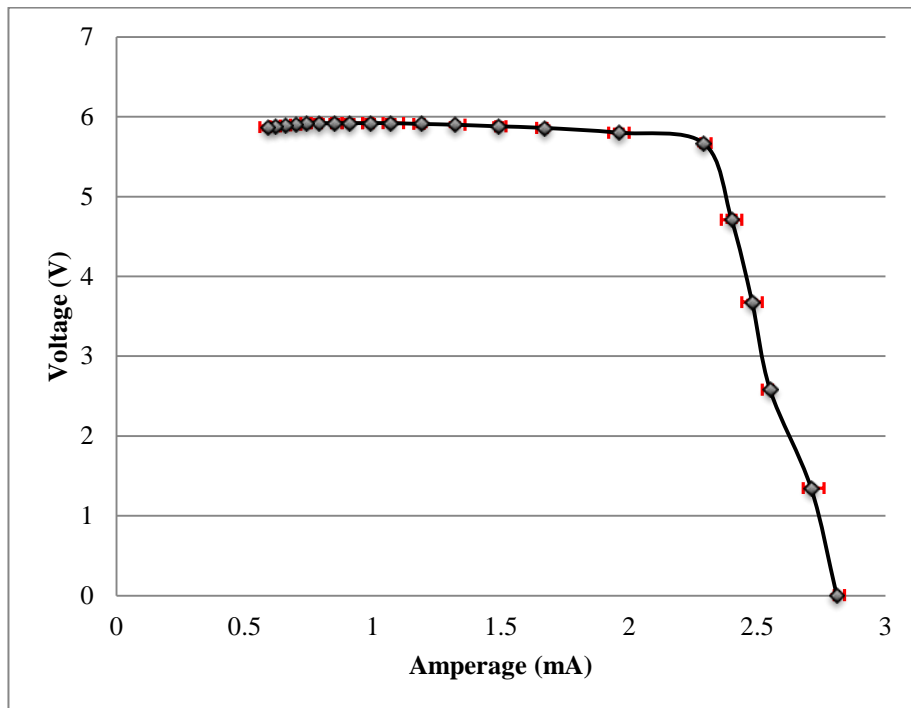


**Figure 24 - I-V Curve for a Single Solar Cell**

Due to time constraints, the team was unable to test a full array, but this would represent the next phase of testing. In preparation for the 2012-2013 MQP, the team built a solar array with four solar cells wired in series. This array was sized to fit the existing Lab Option CubeSat structure and mounted on circuit prototyping board. A quick test of these cells showed that they were properly wired in series, providing somewhere near 25 volts.

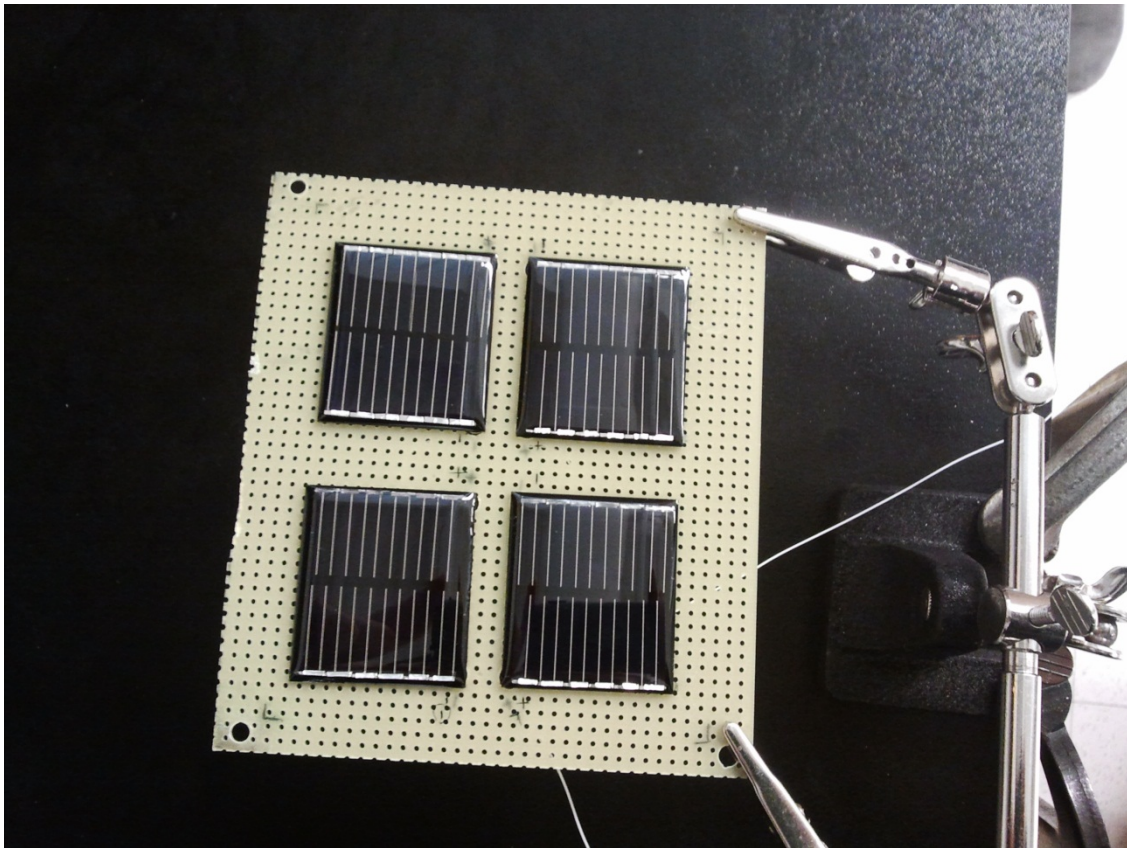


**Figure 25 - Lab Option Solar Array**

## **4. Analysis and Findings**

### **4.1 Mechanical Subsystem**

The random vibrational testing for the structural analysis on our CubeSat was conducted with the SolidWorks Simulation Professional 2012 tool. The test was to simulate typical launch environments where the highest static and vibrational loads would occur on our structure. This included tests for static loads using parameters from typical launch environments and random vibrations using parameters to prepare for worst-case scenarios as documented in GSFC [5]. Tests provide estimates of typical von Mises stress and displacements that could occur in typical launch environments. The structure materials' yield strength would be compared to the results and further investigations on critical regions could be addressed, if needed.

For the SolidWorks Simulation tool to produce the desired results, there were several inputs that fall under the capabilities of this program. There were two study types performed, linear dynamic and random vibration. The linear dynamic mode was used to compute any static loads that occur during the launch environment when the CubeSat is mounted in the launch vehicle. The random vibration mode was used to investigate vibrational loads the structure would endure in typical launch environments. A material must be selected to perform simulations of the structure's behavior, which for this study was the Pumpkin structure consisting of AL 5052-H36. The fixtures for the test structure assumed for our testing constraints were based on the P-POD constraints. The force option selected was "Base Excitation", simulating loads at the top and bottom faces of the CubeSat where the forces would be acting due to the location of mounting points on those faces. The input was the ASD versus frequency curve from the worst-case scenario

launch profile found in NASA’s GEVS document, referenced in Section 2.2.4. This was chosen as the highest load bearing launch vehicle.

We computed the von Mises stress in the SolidWorks Simulation tool. The fixtures were placed at the each of the rails on the bottom and top faces of the structure, as depicted below. This value, when compared to the materials’ yield strength, shows the stress loads the CubeSat endures during the launch. This comparison is important for the structure because if the material chosen cannot withstand the launch loads, the CubeSat will not survive long enough to be deployed.

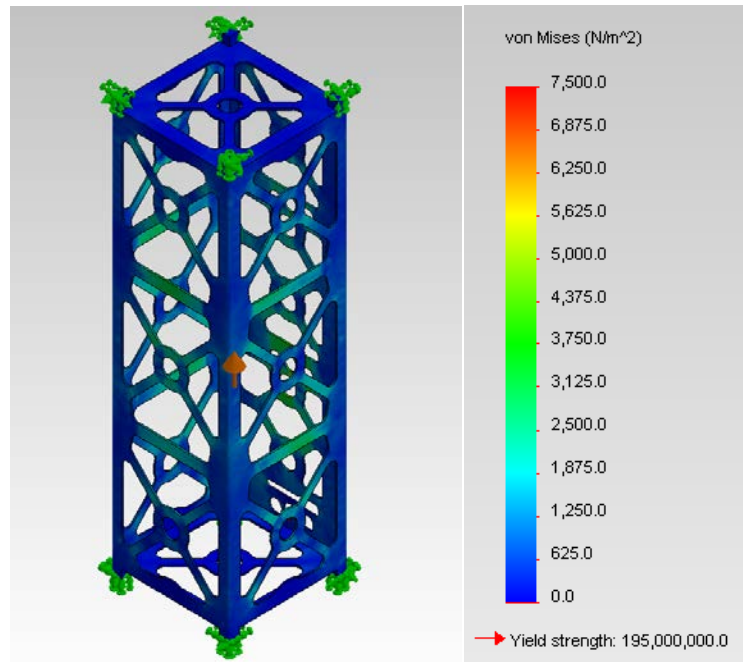


**Figure 26 - Von Mises Stress Output Based on Worst Case Frequency Curve**

The results provided us with von Mises stress varying from  $0 \frac{N}{m^2}$  to approximately  $4000.0 \frac{N}{m^2}$ . Even if the stress had reached the largest value on the scale, approximately  $7500.0 \frac{N}{m^2}$ , the yield strength of the Al 5052-H36 is  $195000.0 \frac{N}{m^2}$ . The areas affected the



most by the von Mises stress occur in the second and middle unit of the CubeSat. The test showed that the material used on the Pumpkin structure, assumed for our CubeSat, should be able to withstand the vibrational loads throughout the launch period for any of the launch vehicles provided likely to be used.

The next area of concern was the deformation that occurs during launch from random vibrations and static loads. If the loads are too great, the structure could deform and cause massive damage to the internal components. SolidWorks was able to produce values for our worst case scenario. The results showed a scaled (x40000) bowing of the structural walls both inward and outward.

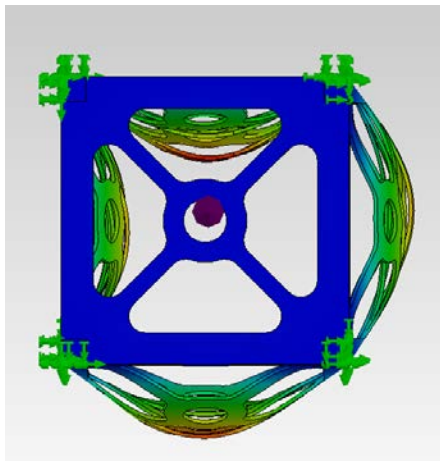


**Figure 27 - Deformation Output Based on Worst Case ASD Curve (x40000 scale)**

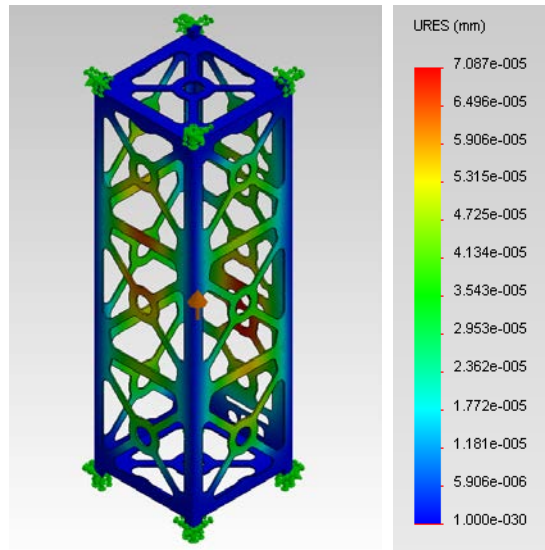


**Figure 28 - Deformation Output Based on Worst Case ASD Curve**

But when the values of the physical deformation are looked at, they only vary from  $1000 \cdot 10^{-30} \text{ mm}$  to  $7.087 \cdot 10^{-5} \text{ mm}$ . These values are extremely small and can be considered negligible with respect to the integrity of the structure during launch, as this set of results represents a worst-case scenario. The critical points of deformation seem to occur once again in the central unit of the 3U structure, but seem to pose no threat as the material is more than strong enough to withstand the loads.

## 4.2 Thermal Subsystem

In the following section we present our analysis on the internal and external modeling of the CubeSat in COMSOL. The sections are presented in the following order:

1. The beginning of our analysis that started with a simplified steady-state study and simplified geometry.
2. The addition of multiple orbits and time-dependent analysis and more complex geometry

3. The completion of our model with the inclusion of the models of internal components.

#### 4.2.1 Steady-State Heating in COMSOL

Our approach to the thermal analysis was to assume that the heat flux from the sun was a constant, and did not vary with time. This allowed us to start with a simpler steady-state model in which only the inward heat flux and surface to ambient radiation would be defined so that a simple model could be viewed.

We started with a simple geometry, which can be seen in Figure 29. This model was made by defining temperature on one of the sides of the CubeSat, which we realized was not enough. We had to define an inward heat flux in order to correctly simulate the effects of the sun's radiation on the body. In addition, this was one of the first models in which we defined the material correctly from the library, which made results more accurate as a result of the correct material properties in place.

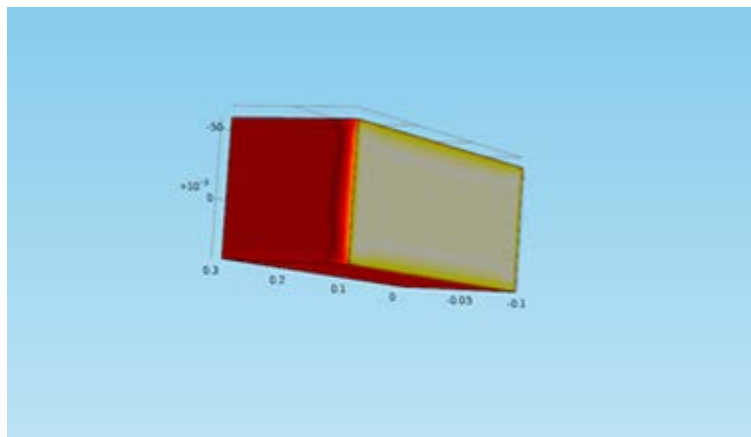


**Figure 29 - Simplified CubeSat Structure**

The next step was to increase complexity of the model and add heat flux, surface to ambient radiation, and conductive boundary layers. We ran into problems with

meshing many of our models. As more complex geometries were imported into SolidWorks, we noticed more mesh errors that prevented equations from being solved.

We found that an effective model should have enough mesh elements to ensure that it is adequately represented, but those elements should not be so fine as to slow down the simulation. In our analysis, we noticed that many mesh errors could be solved by simply decreasing the minimum element size in the mesh creation settings. While this approach was effective for ensuring models would not have errors, they were computationally inefficient. Smaller minimum mesh element sizes meant longer computation times, which led to the inability to test new ideas or add new physics quickly. The key to creating an efficient mesh is to use the “mapped” function, in order to refine mesh elements in specific areas of the CubeSat where problems are occurring.

In the example shown in Figure 30, the joints between the top of the aluminum skeleton and the sides were often an issue in meshing due to their small radii.

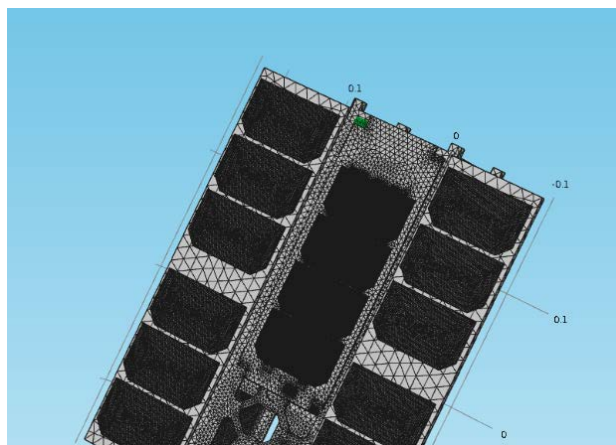


**Figure 30 - Solver Errors**

The dense mesh would often cause solver errors, which would render COMSOL unable to compute the temperature through the satellite. In order to fix these solver errors,

we tried re-importing the models as different file formats which did not help. As a result, much of the thermal analysis done was completed with simpler versions, created by both our Mechanical and Structural Subsystem and Thermal Subsystem teams. These simplified models can be seen in Figure 31.

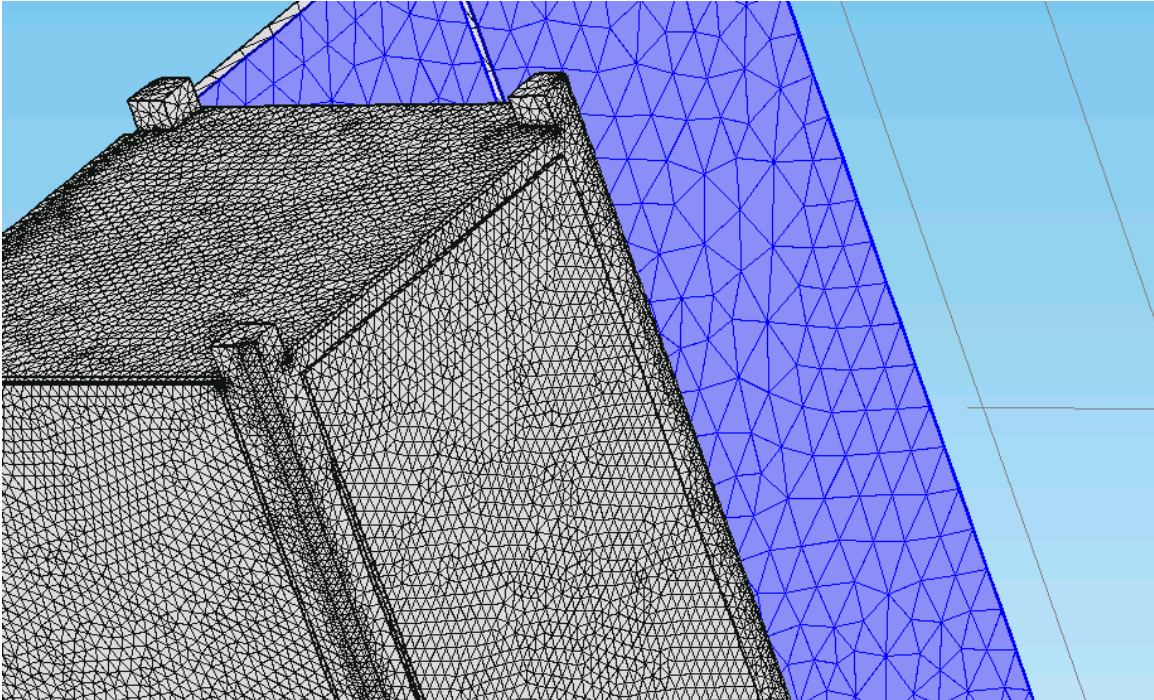


**Figure 31 - Successful Meshing of the Simplified CubeSat Model**

The simpler model of the CubeSat was designed in SolidWorks to closely match the model being created by the Mechanical and Structural Subsystem team. The models were re-created from the ground up in SolidWorks in order to ensure that there were no features or extra parts that were causing errors. The simpler CubeSat model allowed our analysis to continue, and the beginnings of our model were beginning to take shape. The final steady state results are seen in Figure 32.

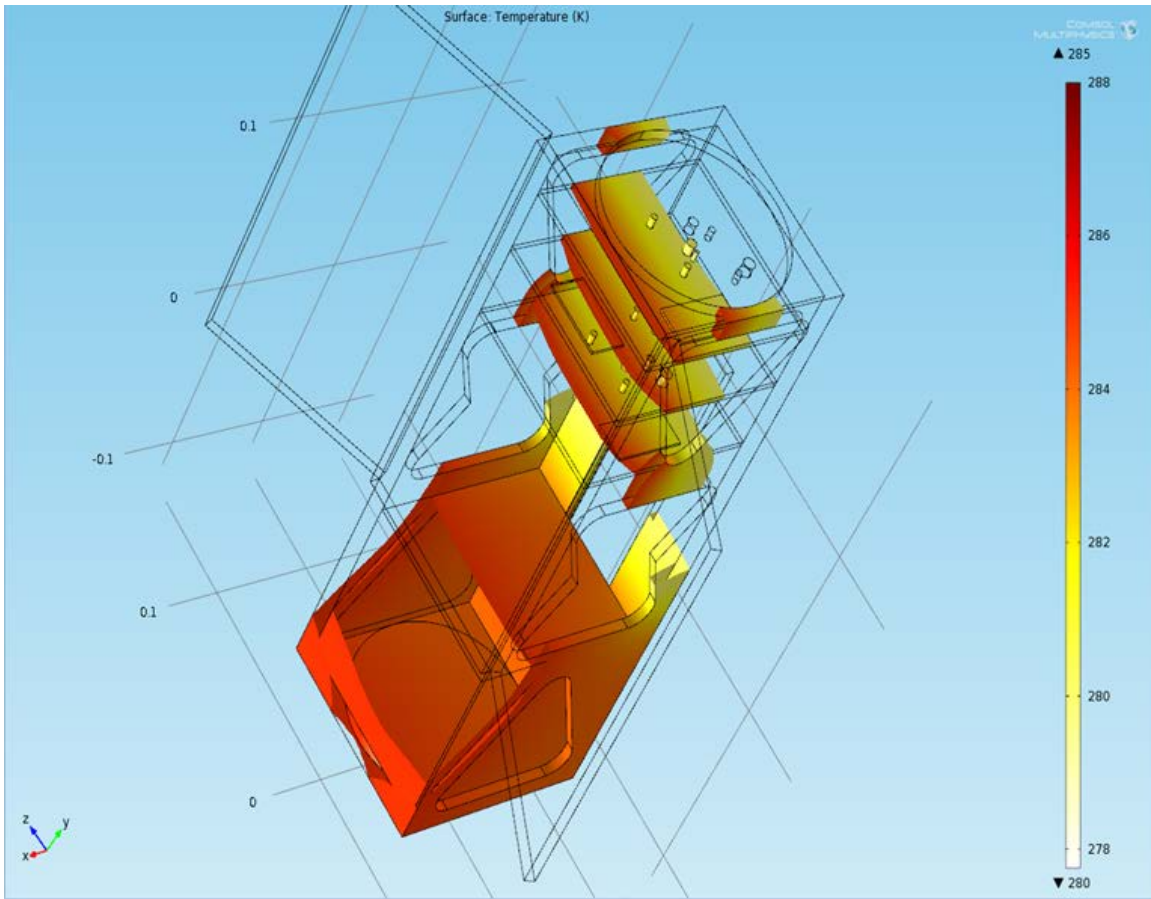


**Figure 32 - Steady-State Thermal Model**

The model in Figure 32 was created as a proof-of-concept, by proving that we could mesh geometries with complex features, and mesh with the addition of assemblies and small elements. In this particular case, the displayed temperature range was changed to show the specific distribution of a certain temperature in the body, which would be useful for isolating locations where the temperature may be above or below required limits.

Once comfortable with the steady-state model, we decided to move on to the more complicated approach of varying the solar flux with time. In the following section, we

detail our analysis of adding a time-dependent study to our COMSOL model in order to compute the effect of multiple orbits.

#### 4.2.2 Multiple Orbits in COMSOL

The next step in our thermal model was to increase the complexity to include orbits that varied with time. Our initial approach to varying the solar flux with time was to generate a series of data points in MATLAB to import into COMSOL's solver. It was planned that COMSOL would be able to take these data points and apply them to the model at specified time steps. Early results can be seen in Figure 33, where the solar flux was to be varied on the face of the CubeSat vs. time.

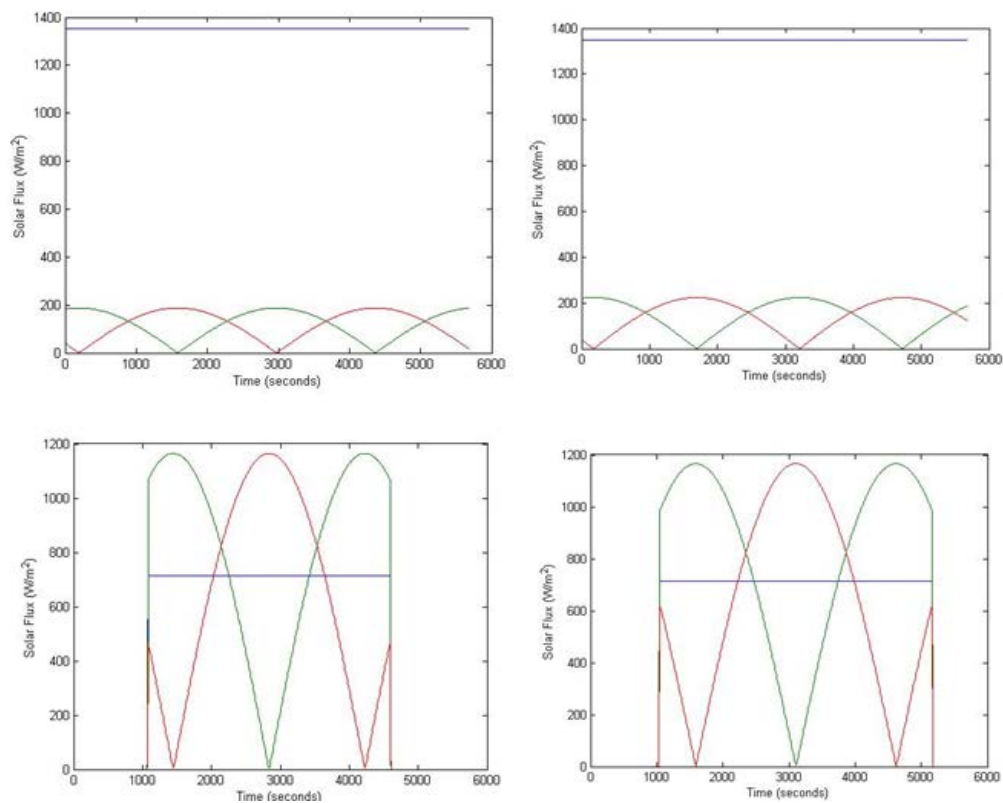


**Figure 33 - Variation of the Solar Flux vs. Time in MATLAB**

We decided importing solar fluxes from MATLAB was unnecessary for several reasons. Due to the sun-synchronous nature of our CubeSat's orbit and the instrument's need to be pointed at the sun with a small margin of error, we determined that the sun-facing surface of the CubeSat would not stray much from being perpendicular to the vectors of the sun's radiation. Importing MATLAB code into COMSOL to use in a time-dependent analysis proved more difficult than previously thought. In order to maintain the ability to vary the sun flux based on possible eclipses, we decided to design an equation in COMSOL that could vary the solar flux.

One of the tasks of our thermal analysis was to analyze if there were trends in multiple orbits between being in direct sunlight and eclipse. Using the equations developed in Chapter 3, we generated several thermal envelopes that showed the heating and cooling over multiple orbits. Initially, we created a thermal envelope over the first 10 orbits for the external components, as the internal components had not been added.

There were several obstacles to overcome with this approach. The method used to compute multiple orbits was time-dependent studies. This involved setting a range of times to perform the study over, and a time step that specified when iterative equations were applied. In order to compute multiple orbits, we specified the total orbital period as 5553.6 seconds, which was supplied by the Mission Analysis team. This number was multiplied by 10 and used as the upper bound in COMSOL's time dependent solver.

The time step was specified in order to ensure that the computation time would not be too long. A time step of one second was used, in order to maintain data with a high resolution. For quicker computations, a larger time step was used to ensure that the final



output would not be an error. Once the simulation was complete, a graph was created by selecting all edges of the spacecraft, and plotting their temperature data vs. time.

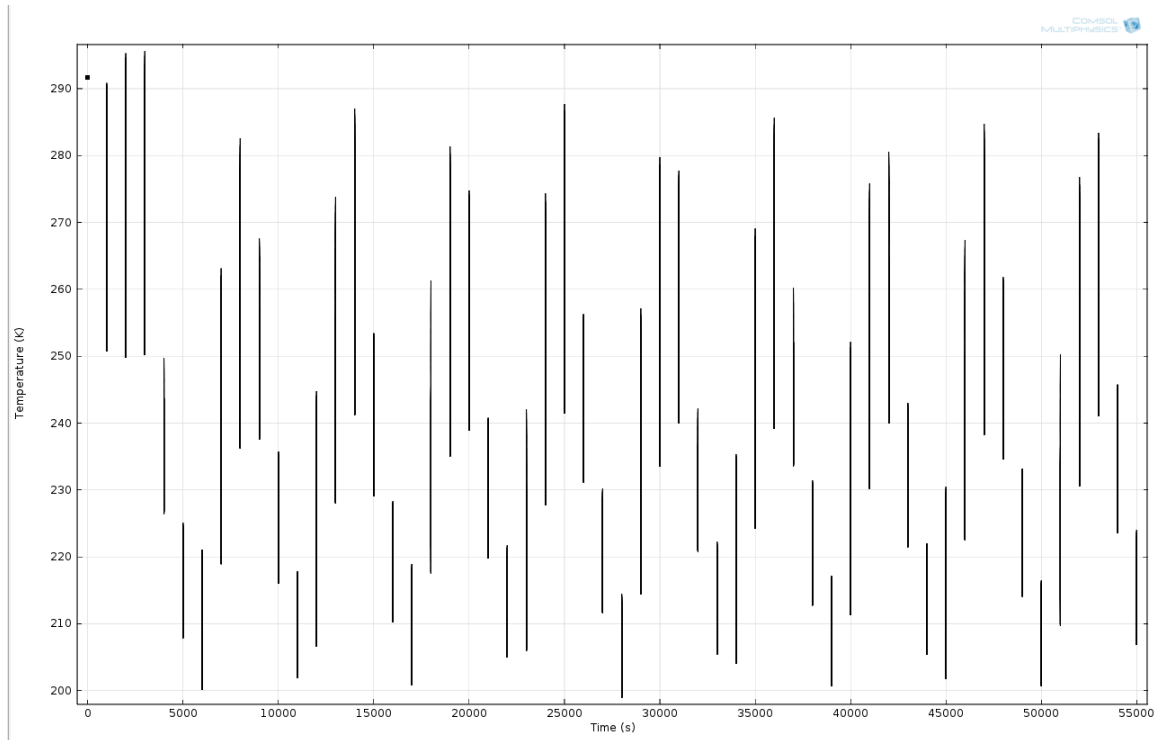


**Figure 34 - Temperature Data vs. Time for 10 Orbits**

This showed data points for every temperature that a given edge had seen during the iterative analysis, plotted in a vertical line over a user-controllable number of orbits (10 in the case of Figure 34). By decreasing the time step, there were many more data points, which resulted in a temperature “envelope” that can be seen in Figure 35. The example shown is for the entire spacecraft, but many different approaches can be used to aid in component selection. By selecting only the edges on the circuit boards, for example, one can create a thermal envelope that will show the maximum and minimum temperatures they will see over the course of many orbits, which will allow the

component selection engineer to select parts that fit within survivable and operational ranges.

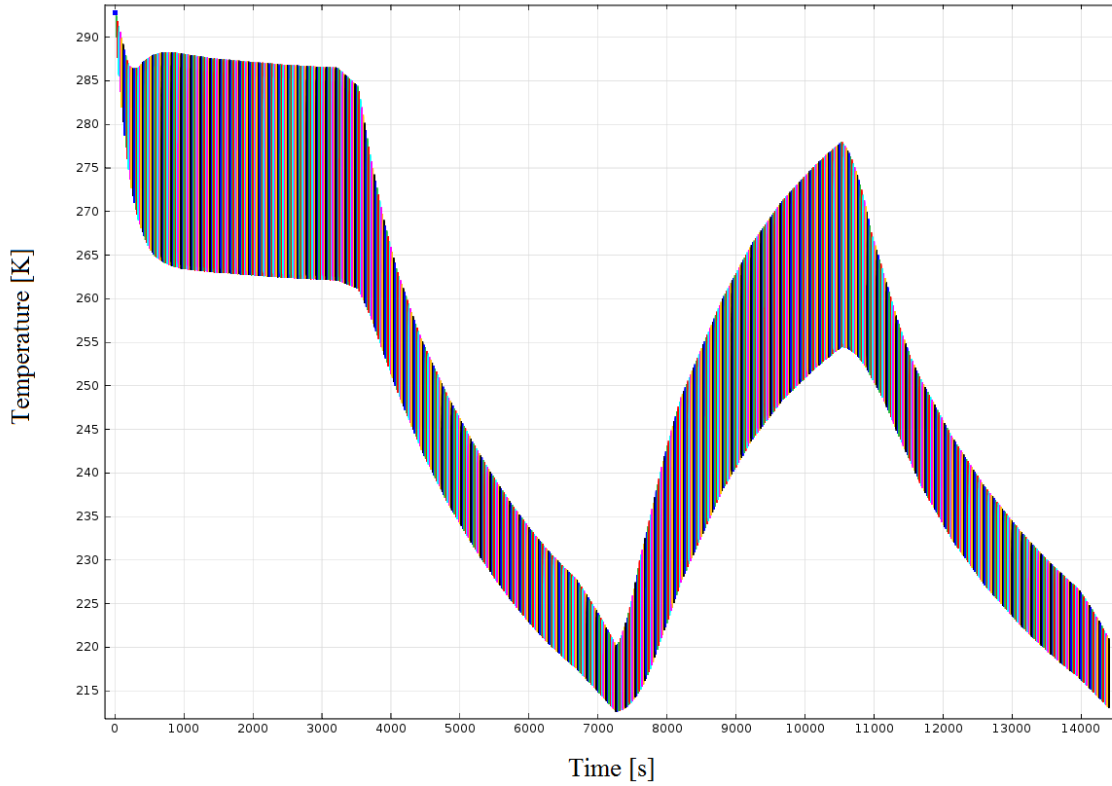


**Figure 35 - Thermal Envelope for External Satellite Components**

In addition, snapshots of specific times could be used to see the thermal distribution of the satellite in eclipse or full sunlight, which can be seen in Figures 36 and 37. In order to better compare the data, COMSOL's output was adjusted to show the same temperature scale regardless of the data being represented.

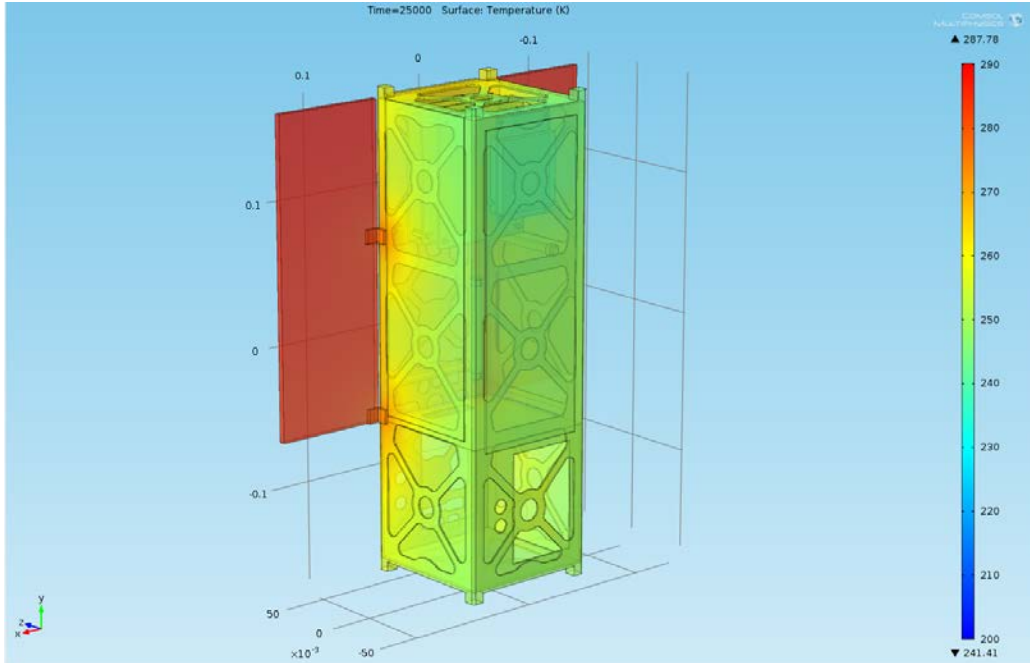


**Figure 36 - Temperature Distribution (in degrees Kelvin) during Full Illumination**

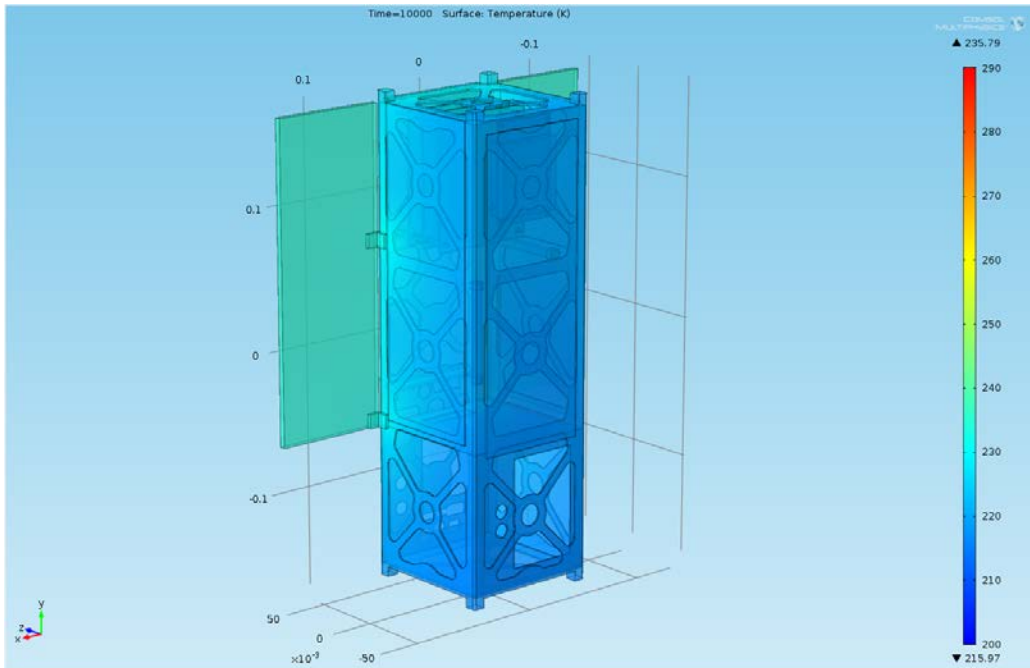


**Figure 37 - Temperature Distribution (in degrees Kelvin) during Eclipse**

These results represent the point where our external thermal analysis had come far enough to begin to add the internal heat generating components to our model. The next subsection details the specifics of their addition.

### 4.2.3 Internal Components

The internal heat components we identified as the most important from a thermal design standpoint and selected for detailed analysis were the battery, EPS, GPS, magnetometer, magnetorquer, OBC, instrument payload, PDM, and sun sensor. Each component was made of different materials and generated a different heat output. The materials and heat generation for each component are outlined in this section.

To determine the heat transfer from each component, we used the efficiency to calculate an estimate of the likely power dissipation. Since these components are made of many individual parts and sub-assemblies, in order to model them we needed to determine an equivalent density and heat capacity for each. Table 5 lists the material properties for all materials assumed in the analysis.

**Table 5 - Component Materials**

<b>Material</b>	<b>Density (kg/m<sup>3</sup>)</b>	<b>Heat Capacity (J/kgK)</b>	<b>Thermal Conductivity (W/mK)</b>	<b>References</b>
Aluminum 6061	2700	950	170	[34]
1.6 mm thick multi-layer PCB	140	409	2.71	[40]
Silicon Dioxide	2150	750	1.5	[35]
steel screws with Zinc plate Clear Chromate finish	7600	490	14.9	[36]
Nickel-Chromium	8400	419	9.9	[37]
Carbon Fiber Casing	1680	754	13	[38]
Aluminum Mounting Brackets	2670	910	239	[34]
Lithium Polymer	530	3450	70	[39]

These properties are needed for COMSOL to accurately determine the amount of heat transferred between the different materials and the total heat transferred by the components. The heat transfers between the solids are determined by Equation 4.1, as defined by COMSOL.

$$\rho C_p \frac{dT}{dt} + \rho C_p u_{\text{trans}} \nabla T = \nabla(k \nabla T) + Q \quad (4.1)$$

Where  $\rho$  is the materials density,  $C_p$  is the material's heat capacity,  $T$  is the temperature,  $k$  is the thermal conductivity of the material,  $Q$  is the energy transferred, and  $u_{\text{trans}}$  is the thermal transmittance between two materials.

All components simulated started with an initial temperature of 273K and as the simulation ran, the heat sources changed the temperature for all components. Table 6 lists the different components, their nominal power consumption, and the assumed efficiencies. The OBC is designed specifically for each satellite, since the efficiency is unknown for this satellite's OBC, the efficiency will be assumed based on the GPS circuit board.

**Table 6 - Internal Components**

<b>Component</b>	<b>Required Nominal Power (W)</b>	<b>Efficiency (%)</b>	<b>Efficiency References</b>
Payload	10	20	
GPS (SGR-05U)	.800	38.4	[41]
Magnetorquer (Zarm Technik AG MTO 2.1 (Power Optimized))	.140	50	[42]
OBC	.300	40	
EPS Board (CS-3UEPS2-N)	13	90	[43]
PDM (CN-USM-5025-DLR-SW)	.16	75	[44]
Battery (CS-3UEPS2-N)	12	90	[45]

The thermal analysis of the internal components was divided into several subassemblies. The first subassembly analyzed was the circuit board stack; this stack included the following components (in order from farthest to closest to the CubeSat side wall): the battery, the EPS, the PDM, and the OBC. We assumed that the heat was only transferred from one board to the other via conduction through the screws. In order to make the model simpler, we also assumed that all of the heat (from a given board) was dissipated from one place on the board. Each of the boards was modeled as a large, multi-layer printed circuit board connected to the others and to the spacecraft by M2.5mm fasteners, which are steel screws with zinc plating and a clear chromate finish. The battery board will have two lithium polymer batteries as heat sources. The other boards will have a silicon dioxide chip to represent the different parts that will produce heat.

The circuit board stack dissipates heat generated by two lithium polymer battery cells mounted on the battery board, and the silicon dioxide cells on the EPS, PDM and OBC. Each of these heat components are simulated as a uniform heat source throughout the whole volume. These heat sources are mounted on a printed circuit board. The circuit

board has dimensions of 90mm x 97mm. The board is then attached to the rest of the stack and the stack to the spacecraft by steel screws with zinc plating. The screws have a height of 10mm and a diameter of 5.3mm. The screws will have the circuit boards separated by 10mm. Based on this analysis the hottest component will be the EPS (See Figure 38). This component will have an average temperature of about 450 K. The stack will have an average heat flux of  $350 \frac{W}{m^2}$  at the base of the screws which will be transferred to the rest of the spacecraft through the mounting screws.

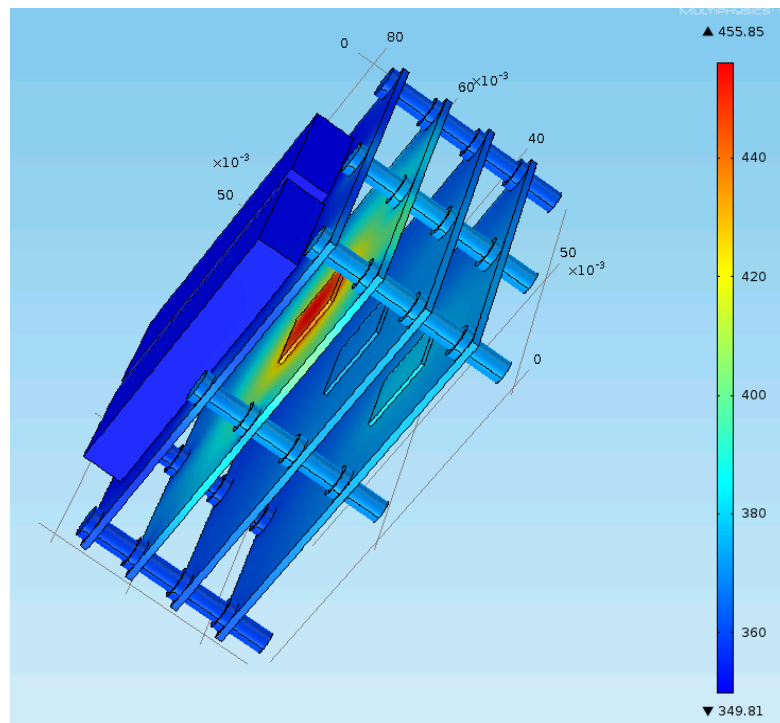


**Figure 38 - Thermal Analysis of the Stack**

Another similar subassembly is the GPS, which is simulated as a single level circuit board. The GPS, was thermally modeled as a single silicon dioxide cell mounted on a circuit board. The silicon dioxide cell was modeled as a heat source distributed uniformly throughout the volume. The board is then attached to the rest of the stack by

steel screws with zinc plating. The board is 70mm by 45mm and the screws have a diameter of 5.35mm and a height of 10mm. The GPS will have an average heat flux of  $10 \frac{W}{m^2}$  at the base of the screws which will be transferred to the rest of the spacecraft through the mounting screws.

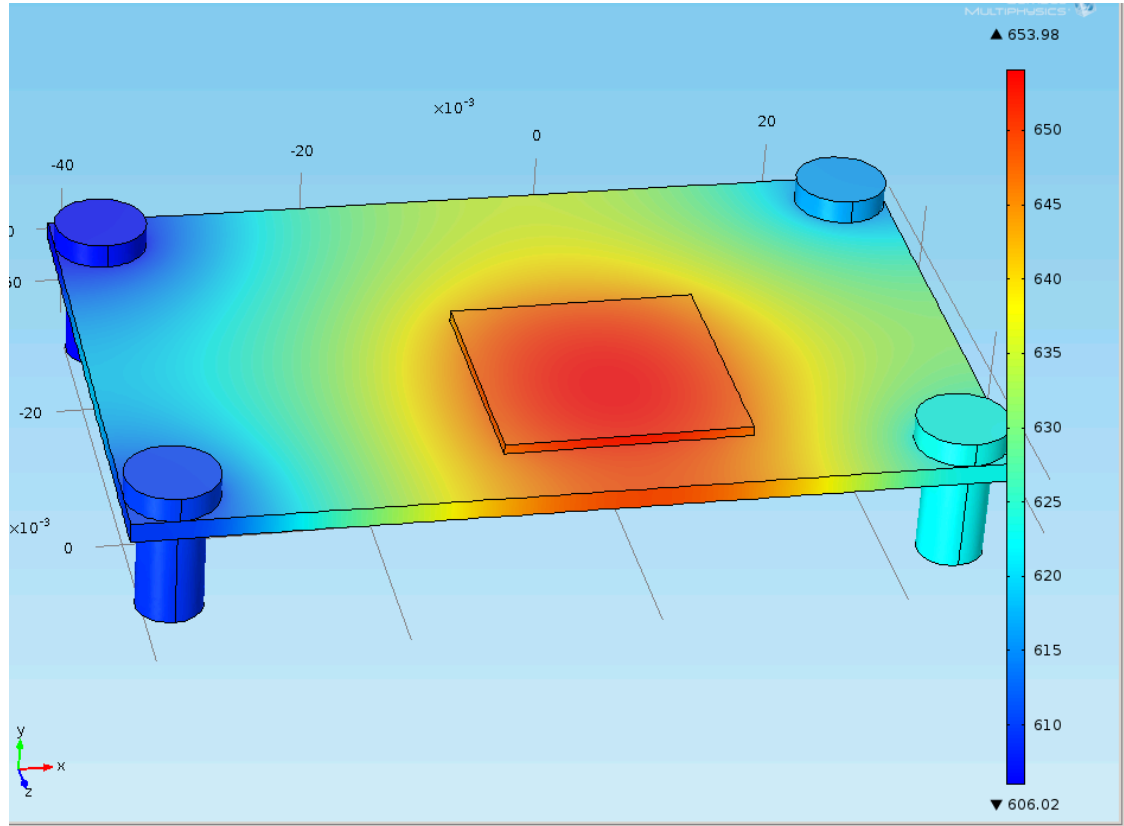


**Figure 39 - Thermal Analysis of the GPS**

The third subassembly modeled was the magnetorquer. The heat is dissipated through a nickel chromium core which comprises the interior of the magnetorquer. The core is surrounded by a carbon fiber plastic casing; the casing was modeled as being directly in contact with the surface of the core. The casing was modeled to be a length of 86mm and a diameter of mm. The magnetorquer is then attached to the spacecraft with aluminum mounting brackets, which have a height of 10mm. The outside of the carbon



fiber casing and the mounting brackets have an average temperature of about 293K. It will dissipate an average of  $10^{-8} \frac{W}{m^2}$  at the base of the aluminum mounting brackets to the satellite sides.

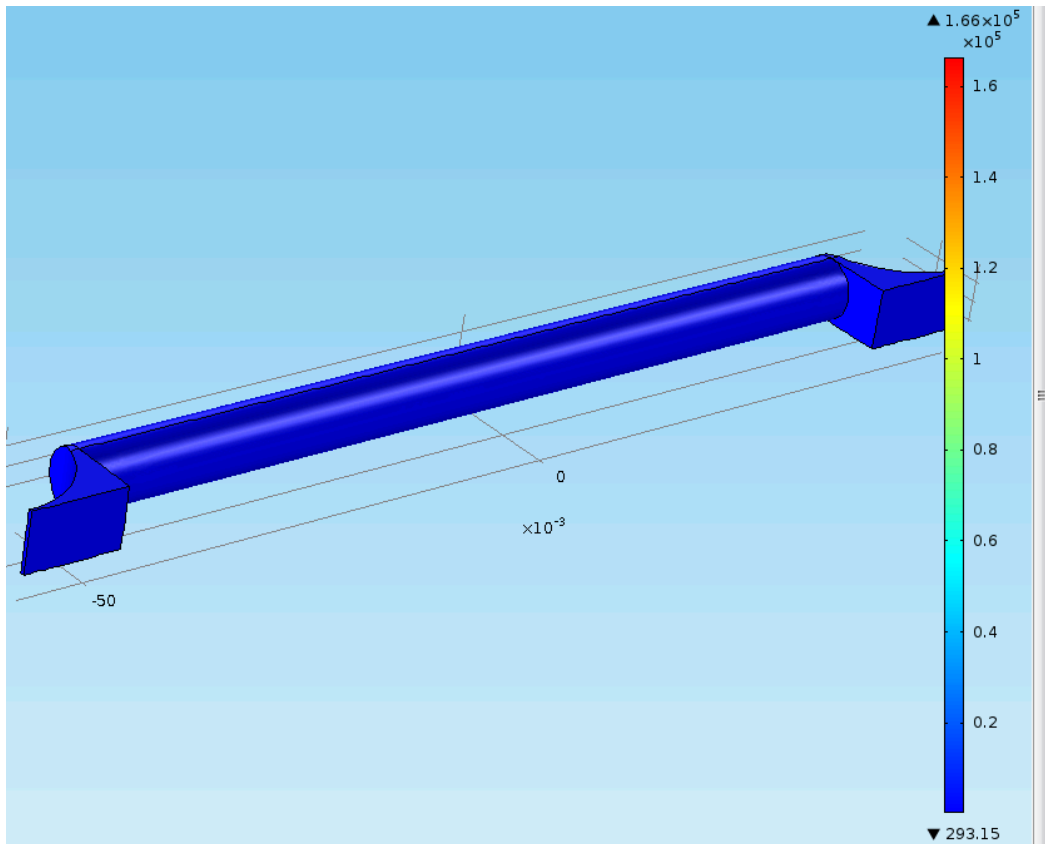


**Figure 40 - Thermal Analysis of the Magnetorquer**

The fourth subassembly modeled was the instrument payload. The payload was approximated as a 1U cube. For this analysis, we were not concerned with the internal components of the payload, just the heat produced by it. We assumed that two of the six sides were radiators that reject a total of 75 % of the heat generated by the internal components. We assumed a worst case, 20 % efficiency for the payload. The payload requires a total of 10W, which means that a worst case requires dissipation of 8W. We assume that the payload box is made out of Aluminum 6061 and will have radiators on

two sides that have radiators that will dissipate 3W each. This means that the remaining four sides will each dissipate 0.5W of heat each. The payload is secured to the rest of the satellite along the edge of the cube. Through these connections the payload will conduct heat to the rest of the satellite. This simulation had little to no impact on this simulation because this simulation was based off of heat fluxes because of the unknown interior components.

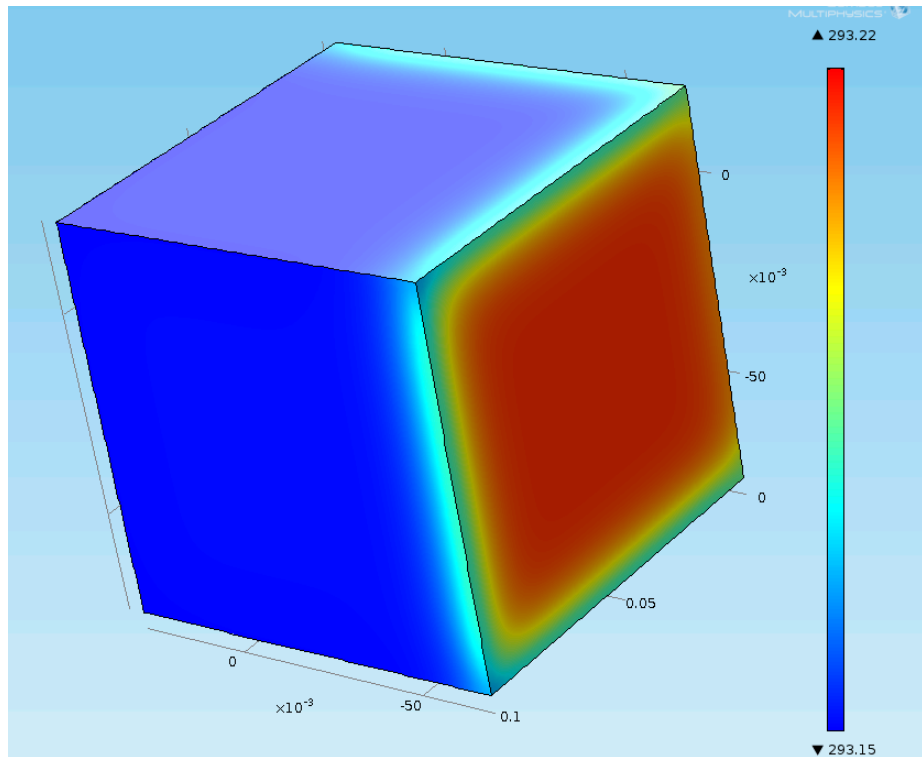


**Figure 41 - Thermal Analysis of the Payload**

After reviewing the power consumption for the magnetometer, we decided to exclude it from our thermal analysis because of the minimal amount of heat that it produces. The magnetometer is assumed to be 90 % efficient and requires a maximum of 14.85mW during operation [46]. As a result, the amount of heat dissipated is 1.5mW. This amount of heat dissipation is negligible compared to other components.

Lastly, it is important to note that the sun sensor requires no power to be supplied to it and generates its own power from the sun. For this reason it was not listed in Table 6. The power generated is a maximum 50mW. The efficiency of the sun sensors and most photodiodes are 80 % or above [47]. This means that the maximum amount of heat dissipated is 10mW. This level of heat dissipation over a small area has very little impact on the overall thermal balance of the spacecraft and was considered negligible.

The next subsection details the analysis and what we have found from setting up the laboratory verification of COMSOL, as outlined in Chapter 3.4.3.

#### **4.2.4 Lab Option Verification**

Due to time constraints, we were unable to finish the lab verification of COMSOL results as outlined in the methodology chapter, but were able to set the framework for future groups to verify COMSOL results. This will be accomplished by conducting experiments in the vacuum chamber using a LabView Virtual Instrumentation (VI) program, a collection of thermocouples, and a data processing unit. The LabView VI has been constructed and tested using a single thermocouple outside of the vacuum. The VI has been created with functionality allowing the adjustment and modification of several experimental parameters including; thermocouple material composition, switching data channels, and the expected minimum and maximum range expected. In addition, the VI has a graphical representation of the temperature at each measurement location and the option to write the results to an Excel sheet.

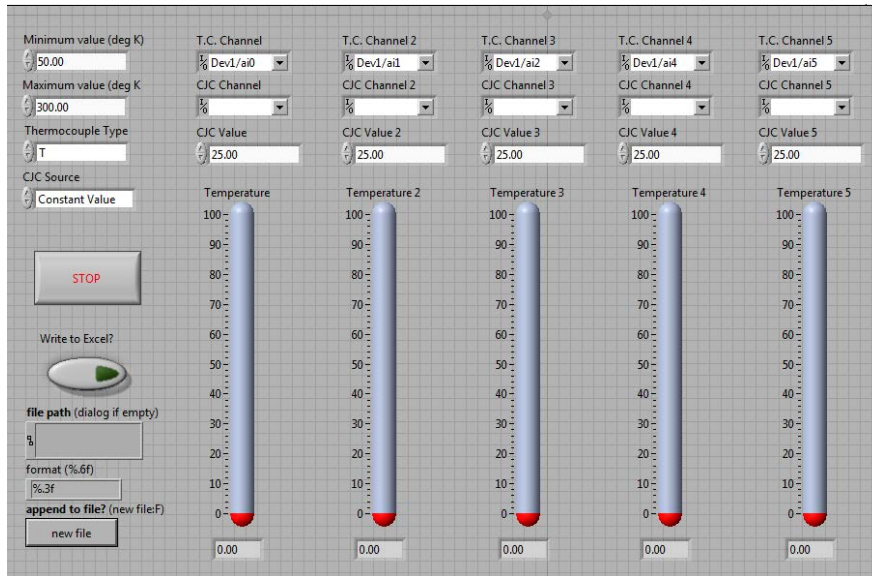


Figure 42 - LabView VI Front Panel

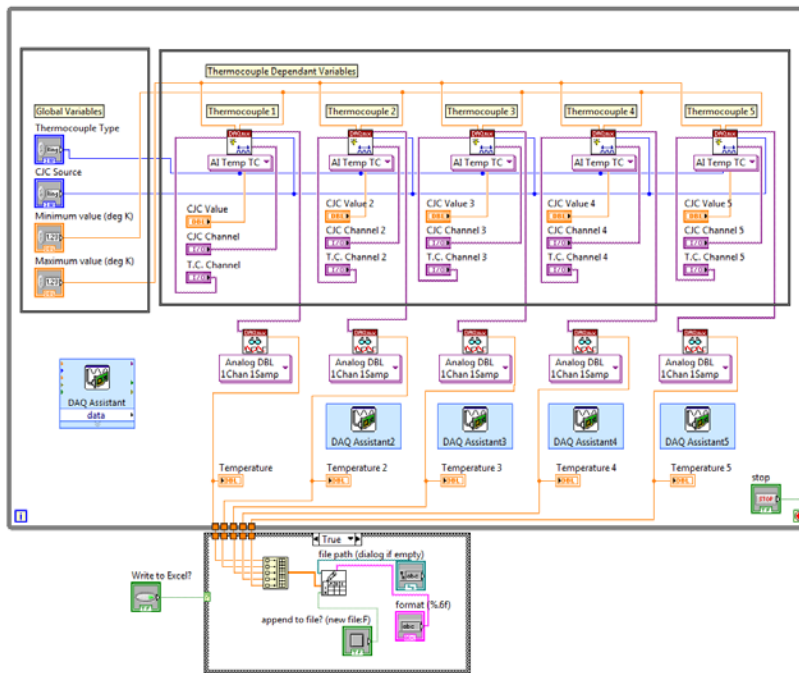
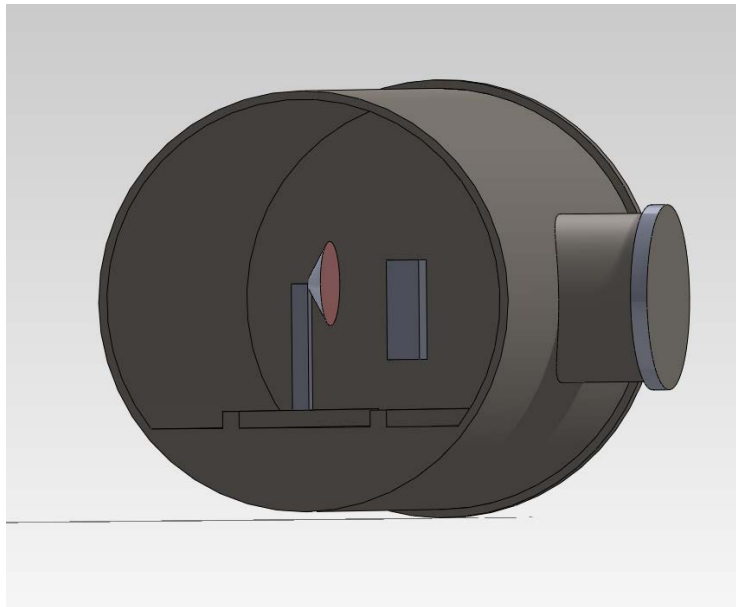


Figure 43 - LabView VI Block Diagram

However, due to the temperature range expected inside the test environment, calibration of the VI may be needed in order to produce accurate results. Once calibrated, the five thermocouples should be placed at locations of interest throughout the chamber depending on which area of the COMSOL model is being verified. The following is a basic model of the expected configuration of the test chamber that was used when considering placement of thermocouples, however at the time of creation the test stand had not been designed by the Mechanical and Structural Subsystem.



**Figure 44 - Basic Vacuum Chamber CAD Model**

In Figure 45, the expected temperature distribution of the model is shown in a plot of temperature vs. time. Each point on the graph corresponds to a temperature at a specific edge chosen on the model. Should the laboratory model be tested, the results found from the thermocouples in a similar spot could be compared to these results found on the COMSOL model.

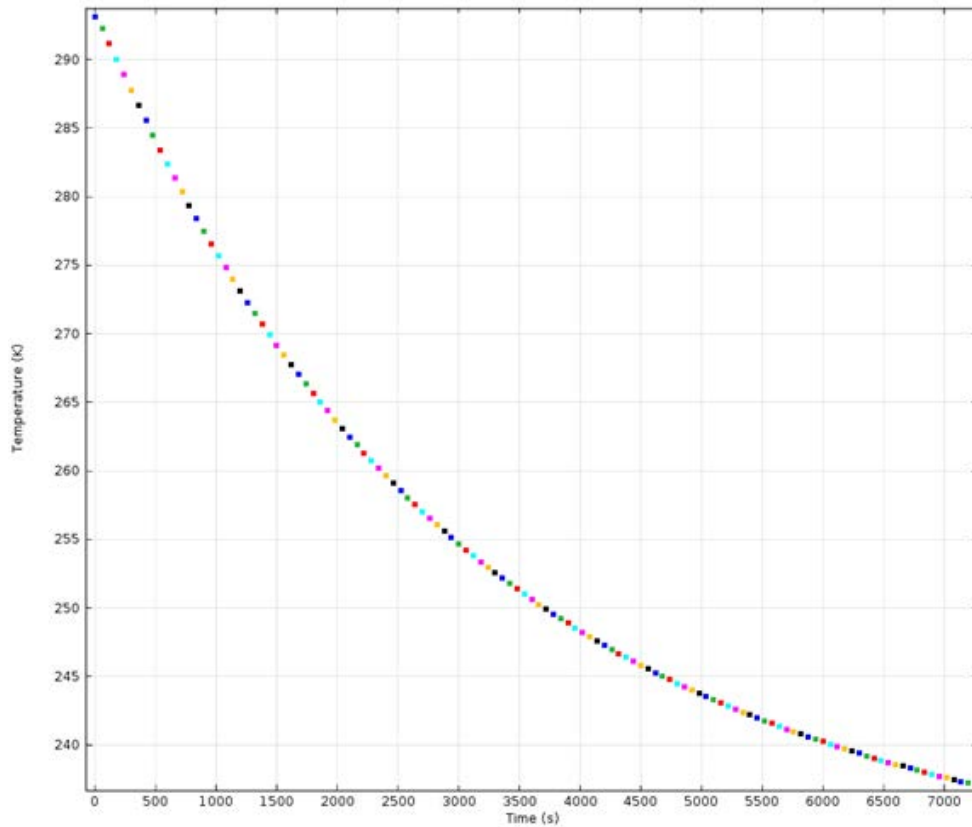


**Figure 45 - Temperature of CubeSat during Simulated Cryopump Operation**

### 4.3 Power Subsystem

Since the power subsystem is integral to almost every other system within the satellite, its components are typically chosen to suit the needs of every other subsystem. For our project, we would need to make three primary choices: The type of PMAD system, the specific components of the PMAD system and the solar panels. Each choice was made according to the demands of the components needed by the other subsystems and their reliability as suggested by their flight heritage.

As mentioned in Chapter 2, there are several choices for a PMAD system. Among these are direct power systems, custom PMAD systems and vendor-purchased PMAD systems. For our application, we were primarily concerned with the reliability of the

system, as it is a common point of failure [28]. Since custom PMAD systems would either require a dedicated flight test or fly untested, they were ruled out immediately. Similarly, direct power systems can be risky due to the lack of controls in power distribution. In addition, our CubeSat would employ magnetorquers for attitude determination and control. By nature of their operation, these actuators require a variable power supply. Vendor-purchased systems, however, have both been flight tested and include controls to provide specific voltages and turn on or off components.

As a result, we decided to opt for a vendor-purchased system. To develop a complete system, would need some form of power control as well as a battery to store power. Once again, reliability and flight heritage would be our primary deciding factor. We found that ClydeSpace systems offered a complete PMAD system consisting of both an EPS and a PDM. These components have flown on many CubeSat missions and provided the control we would need for our components. In addition to this flight heritage, both components included overcurrent protection and were customizable upon request. Since these components were designed to be used together, they also interface easily. ClydeSpace also sells a battery specifically designed for the EPS and PDM in sizes ranging from 10 to 30Whr.

Finally, our solar panel selection was primarily driven by a combination of power and geometric demands. Not only did the solar panels need to provide enough power to sustain each component on the satellite, they would also need to be shaped such that they did not interfere with the instrument or attitude control hardware. Due to this, our solar panels would be restricted to a 2U size. For the purpose of power budgeting, our instrument had been allocated a power of approximately 12W, while the other

components were allocated approximately 1W. As such, it was decided to use an array that consisted of one 2U panel and two deployable 2U panels. This choice provided approximately 16W. Once data for the instrument was received, it was determined that this amount of power may be insufficient. If this is the case, it would be necessary to use ClydeSpace's double deployable panels to add an extra two panels to each side.



## 5. Conclusions and Recommendations

### 5.1 Mechanical Subsystem Conclusions and Recommendations

The members of this project decided to go forward with a Lab Option to do testing on various subsystems, specifically thermal and power, in WPI's vacuum chamber. For this Lab Option, it is recommended that the test structure be completed as well as the connecting adapters for the top and bottom of the CubeSat.

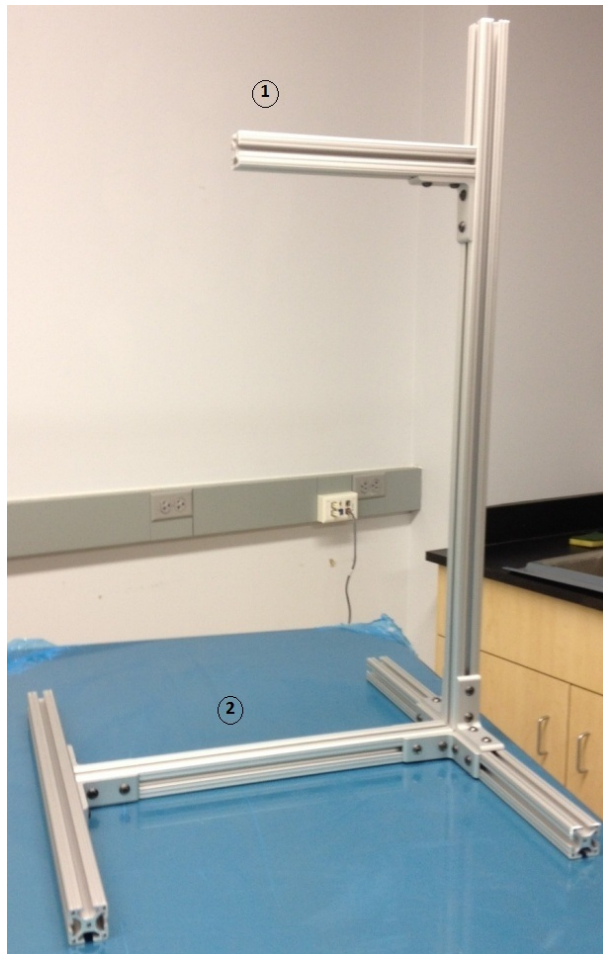


**Figure 46 - Test Fixture**

The structure needs to be completed by drilling holes in the top and bottom “cross-bars”, labeled 1 and 2 in Figure 46, for threaded rods (the holes need no threading). The threaded rod will be held in place by nuts both above and below the

extruded aluminum, as shown in Figure 47. A small hole would need to be drilled for attaching the monofilament line to the threaded rod. With the monofilament line being stretched between the CubeSat connecting adapters, this setup gives the user freedom to make small adjustments to put the monofilament line in tension by simply tightening either of the nuts. This configuration is shown in Figure 47:

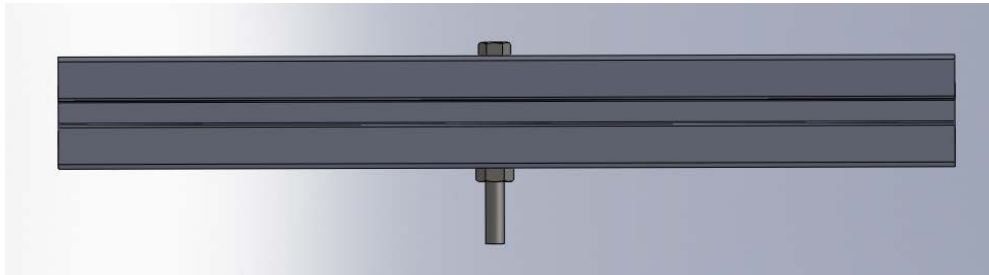


**Figure 47 - Configuration of Threaded Rod**

Figures 48 and 49 show a suggested design for the connecting adapters that attach to the CubeSat model to be made at WPI's rapid prototyping machine; threaded holes would be drilled near the corners on each side for set screws to hold the structure in place. The connecting adapters would attach to the monofilament line via a hook (not pictured) on the top which in turn is tied onto the threaded rods both at the top and bottom.

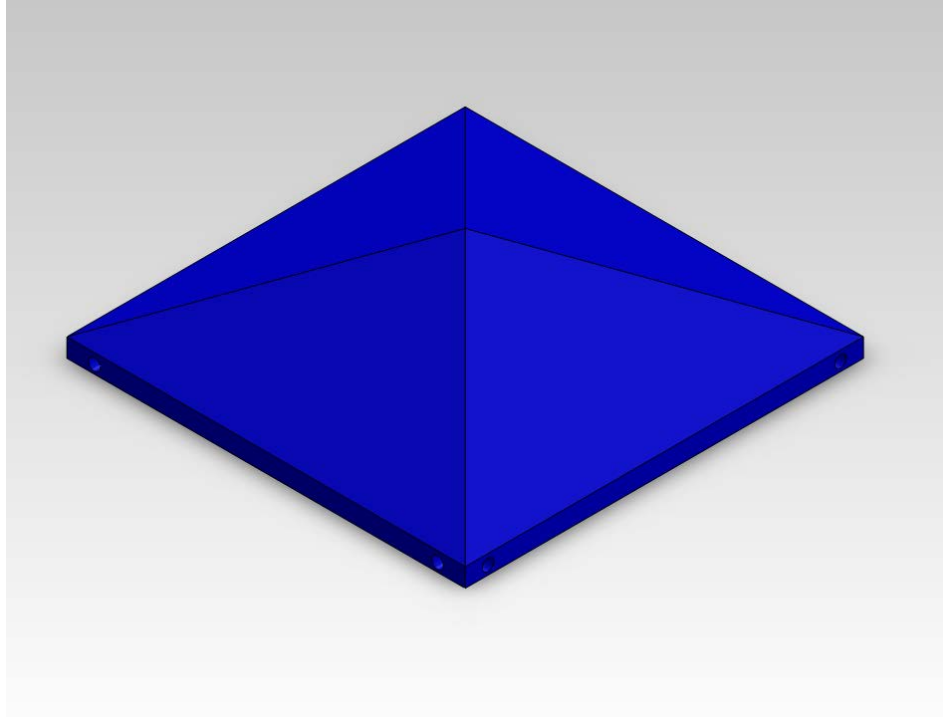


**Figure 48 – Top View of Connecting Adapters**

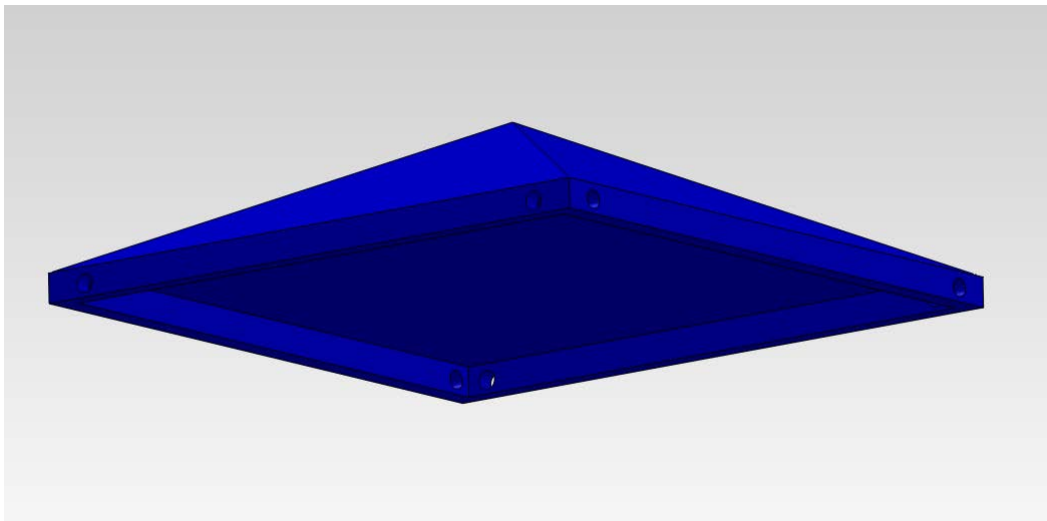


**Figure 49 - Bottom View of Connecting Adapters**

For the Flight Option CubeSat, it is recommended that the 3U structure from Pumpkin be purchased rather than building one at WPI or a local fabricator. While fabricating a structure at WPI would cost less, Pumpkin offers structures through their CubeSat Kit that have been evaluated using random vibration analysis and that also have

flight heritage. It is also recommended that solar arrays be bought from ClydeSpace because they offer a variety of solar panels that are built to be compatible with the Pumpkin structures. ClydeSpace offers 2U and 3U deployable solar arrays that simply flip out from the side of the satellite and also solar arrays

## **5.2 Thermal Subsystem Conclusions and Recommendations**

The following section will detail the conclusions and recommendations we came to from our analysis. Several methods of thermal management exist as discussed in Chapter 2. The Flight Option satellite will most likely depend on passive methods of heat transfer, with the exception of the instrument payload. Most likely, we will use a combination of several strategically placed surface coatings and internal insulation. It would be advantageous to choose a surface coating that responded to the thermal needs of the spacecraft.

The multiple orbital analyses in COMSOL indicated that we would not see much variation in the temperature after the first orbit has been completed. Future MQP groups should consider studying the initial conditions the CubeSat will encounter in the moments before ejection from the P-POD as that temperature had a significant impact on predicted values.

Our thermal model in COMSOL helped us to determine worst case temperature ranges and how the flux varies across the body of the spacecraft. This rudimentary model combined with our preliminary assumptions about the power consumption and efficiency of the payload allows our team to draw an initial conclusion. This would call for the other major heat generating components to be as far from the payload as possible. This placement makes thermal management a more straightforward task as the distance helps

to isolate the systems with the potential for a radiator or other method of thermal outflow in between the two heat sources. When the rest of the team is considering their component selection, the survivability and operating temperatures should be considered a high figure of merit.

In conclusion, with respect to thermal management; spacecraft components should be intelligently selected with largely overlapping temperature ranges and no extreme outliers. Once component requirements and energy outputs are known the thermal team can ensure mission survival. This would be done with the heritage proven and vendor purchased insulation and surface coatings that analysis based on the work performed as part of this MQP will deem necessary.

### **5.3 Power Subsystem Conclusions and Recommendations**

The final iteration of the 2011-2012 CubeSat Flight Option power system design resulted in the selection of the following components (Figure 50):

- Three (3) 2U solar panels
- One (1) Electrical Power System (EPS)
- One (1) Power Distribution Module (PDM)
- One (1) EPS-mounted ClydeSpace battery

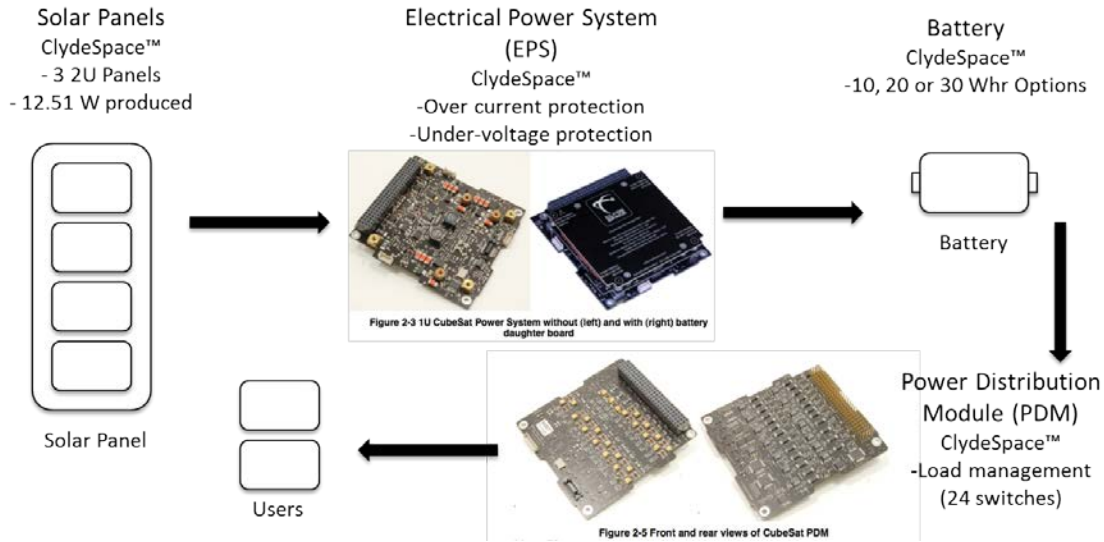


**Figure 50 - Power System Flow Cartoon**

Although there are other power options available, this is the best commercially available power system for our project. ClydeSpace products have extensive flight heritage. The components are also some of the best available, using Spectrolab’s high efficiency solar cells for the solar array and the latest Li-ion battery technology. By using one supplier, we assured that all the components can be easily integrated. These components easily work together to supply and regulate power for the entire CubeSat.

Our team began initial testing for the Lab Option of the CubeSat design. We verified that all components were functional and constructed a four-cell solar array. The solar cells are connected in series to provide the maximum voltage. The 2012-2013 CubeSat design team can continue testing with this array. Possible tests include: generating an I-V curve, determining the effect of the angle of incidence on the array and thermal-vacuum testing. The procedures for generating an I-V curve are outlined in Solar Cell Baseline Testing (3.5.3) where we describe use of this method to characterize a

single cell. Additional testing with the solar array could verify the analytical solutions that we calculated over the course of this project.

## References

- [1] CubeSat.org [homepage on the internet], “Mission Statement” [updated 2011; cited 5 December 2011]. Available from: <http://www.cubesat.org/index.php/about-us/mission-statement>
- [2] Cote, K et al. “Mechanical Power and Propulsion Design for a CubeSat.” MQP Report. Department of Mechanical Engineering, Worcester Polytechnic Institute, Worcester, MA, 2011.
- [3] Heidt, H. “CubeSat: A new Generation of Picosatellites for Education and Industry Low-cost Space Experimentation,” 14th Annual/USU Conference on Small Satellites
- [4] Cal Poly SLO. “CubeSat Design Specification Rev. 12”, The CubeSat Program.
- [5] Harper, A, Ryschkewitsch, M, Obenschain, A, Day, R. “General Environmental Verification Standard,” April 2005. [<http://standards.gsfc.nasa.gov/gsfcd-std/gsfcd-std-7000.pdf>. Accessed 12/7/2011]
- [6] Pumpkin Inc. (2008). CubeSat Kit. Retrieved December 4, 2011, from [cubesatkit.com: http://www.cubesatkit.com/index.html](http://www.cubesatkit.com/index.html)
- [7] ISIS. (2010). Innovative Solutions in Space. Retrieved December 5, 2011, from [isispace.nl: http://www.isispace.nl/index.php?option=com\\_content&task=view&id=61&Itemid=68](http://www.isispace.nl/index.php?option=com_content&task=view&id=61&Itemid=68)
- [8] AAU CubeSat – University of Aalborg (Denmark). Retrieved December 4, 2011, from [cubesat.auc.dk: http://www.space.aau.dk/cubesat/](http://www.space.aau.dk/cubesat/)
- [9] Stras, L., Kekez, D.D., Wells, G.J., Jeans, T., Zee, R.E., Pranajaya, F., and Foisy, D. “The Design and Operation of the Canadian Advanced Nanospace experiment (CanX-1).” Report. University of Toronto Institute for Aerospace Studies, Ontario, Canada (2004) Retrieved December 5, 2011 from <http://utias.sfl.net/nanosatellites/CanX1/CanX1system.html>
- [10] Indian Space Research Organisation (ISRO). 2008. Rincon 9.1. Retrieved December 6, 2011, from [isro.org: http://www.isro.org/scripts/disclaimer.aspx](http://www.isro.org/scripts/disclaimer.aspx)
- [11] *ANSYS Blog | Realize Your Product Promise*. ANSYS. Web. 09 Nov. 2011. <<http://blog.ansys.com/>>.
- [12] *ANSYS Structural Analysis Guide*. Tech. ANSYS, Apr. 2009. Web. <[www1.ansys.com/customer/content/documentation/120/ans\\_str.pdf](http://www1.ansys.com/customer/content/documentation/120/ans_str.pdf)>.



- [13] Bendat, J. S. *MSC/NASTRAN Random Vibration Analysis and Applications*. Los Angeles, CA: MacNeal-Schwendler Corporation, July 1987. Print.
- [14] "MSC Nastran for Integrated, Multidiscipline FEA Solution." *MSC Nastran*. MSC Software Corporation. Web. 12 Nov. 2011.  
<<http://www.mscsoftware.com/Contents/Products/CAE-Tools/MSC-Nastran.aspx>>.
- [15] "Random Analysis of a Simple Structure." *MSC/NASTRAN Application Manual*. Los Angeles, CA: MacNeal-Schwendler Corporation, April 1982. Print.
- [16] Barbela, Mohan. *Random Analysis in Using MSC/Nastran ISHELL Module*. Tech. MSC/Nastran. Web. 12 Nov. 2011.  
<<http://www.mscsoftware.com/support/library/conf/auc97/p04897.pdf>>.
- [17] Wertz, J. R., & Larson, W. J. (Eds.). (1999). *Space Mission Analysis and Design* (3rd Edition ed.). New York, NY; Hawthorne, CA: Springer; Microcosm Press.
- [18] CubeSat. (2010). Past Launches. Retrieved November 11, 2011 from [www.cubesat.org](http://www.cubesat.org): <http://www.cubesat.org/index.php/missions/past-launches/17-dnepr-launch-2>
- [19] CubeSat. (2009). Testing. Retrieved December 6, 2011 from [strath.ac.uk: http://me-wserver.mecheng.strath.ac.uk/group2009/d/testing\\_page.html](http://me-wserver.mecheng.strath.ac.uk/group2009/d/testing_page.html)
- [20] Diaz-Aguado, M. "Small Satellite Thermal Design, Test, and Analysis", University of Texas at Austin.  
[[http://fastrac.ae.utexas.edu/documentation/Diaz\\_Aguando\\_10.1109.pdf](http://fastrac.ae.utexas.edu/documentation/Diaz_Aguando_10.1109.pdf). Accessed 12/7/2011]
- [21] Gilmore, D. "Chapter 2: Spacecraft Thermal Environments".  
[<http://www.globalspec.com/reference/26420/203279/chapter-2-spacecraft-thermal-environments>. Accessed 12/13/2011]
- [22] Spremo, S. "Low Cost Rapid Response Space Spacecraft (LCRRS)." Report. NASA Ames Research Center. Retrieved December 5, 2011 from <http://my.wpi.edu>
- [23] Griffin, M, French, J. "Space Vehicle Design Second ed.", 2004.  
[[http://books.google.com/books?id=31GqndM3fk8C&pg=PA436&lpg=PA436&dq=space+thermal+environment&source=bl&ots=9R6EghTs6X&sig=RZecIBTasfBVkAIG1WlhGxW-E1M&hl=en&ei=BsnfTpm8HKTh0QHoqNmgBw&sa=X&oi=book\\_result&ct=result&resnum=7&ved=0CE4Q6AEwBg#v=onepage&q=space%20thermal%20environment&f=false](http://books.google.com/books?id=31GqndM3fk8C&pg=PA436&lpg=PA436&dq=space+thermal+environment&source=bl&ots=9R6EghTs6X&sig=RZecIBTasfBVkAIG1WlhGxW-E1M&hl=en&ei=BsnfTpm8HKTh0QHoqNmgBw&sa=X&oi=book_result&ct=result&resnum=7&ved=0CE4Q6AEwBg#v=onepage&q=space%20thermal%20environment&f=false). Accessed 12/7/2011]

[24] University of Tennessee Dept. of Physics and Astronomy. The Cosmic Background Radiation. [<http://csep10.phys.utk.edu/astr162/lect/cosmology/cbr.html> Accessed 12/8/2011]

[25] Savage, Chris J. *Spacecraft Systems Engineering 4<sup>th</sup> edition*. 2011, John Wiley & Sons.

[26] Brown, Charles D. *Elements of Spacecraft Design*. 2002, American Institute of Aeronautics and Astronautics

[27] J. den Haan, Solar Power Information. 2009. <http://www.solarpower2day.net/solar-cells/efficiency/>

[28] Clark, C., Strain, A., Mazarias, A.L., "A High Performance, Very Low Cost Power System for Microspacecraft," *Eighth European Space Power Conference*, University of Applied Science, Konstanz, Germany, 2008, pp. 1-11.

[29] "CubeSat | Small Satellite | Nanosatellite | Power | Batteries | Solar Panel | DC DC Converter | CubeSat Shop | Spacecraft" ClydeSpace Ltd., Glasgow, Scotland October 2011. [<http://www.ClydeSpace.com>. Accessed December 18, 2011.]

[30] Rotteveel, J., Aalbers, G.T., Bonnema, A.R., van Breuklen, E.D., Doorn, J.H., van den Eikhoof, R., Van Der Linden, E., Hamaan, R.J., Verhoeven, C.J.M., and Monna, G.L.E., "Delfi-C3: a Student Nanosatellite Test-Bed for in-Orbit Demonstration of Micro Systems Technology." Delft University of Technology, The Netherlands. Retrieved December 5, 2011 from <https://escies.org/download/webDocumentFile?id=1678>

[31] Hoyt, R., and Twiggs, R., "The Multi-Application Survivable Tether (MAST) Experiment." Report. Stanford University, Stanford, CA. Retrieved December 5, 2011 from [www.tethers.com/papers/MASTJPC2003Paper.pdf](http://www.tethers.com/papers/MASTJPC2003Paper.pdf)

[32] Imai, K., Miyashita, N., Iai, M., Omagari, K., Asami, M. Miyazawa, W., Yabe, H., Miyamoto, K., Usuda, T., Fujiwara, K. Masumoto, S. and Matunaga, S. "Tokyo Tech Small Satellite Development Projects." Report. Tokyo Institute of Technology, Tokyo, Japan. Retrieved December 5, 2011 from [http://lss.mes.titech.ac.jp/ssp/cute1.7/subsystem\\_eps\\_e.html](http://lss.mes.titech.ac.jp/ssp/cute1.7/subsystem_eps_e.html)

[33] Wu Zhifei; You Zheng; Salvignol, J. "Tsinghua-1 Micro-satellite power system architecture and design," *Power Electronics and Motion Control Conference, 2000. Proceedings. IPEMC 2000. The Third International*, vol.3, no., pp.1045-1049 vol.3, 2000F

[34] Fortescue, P. W. and Swinerd, G. G. (2011) Attitude Control, in *Spacecraft Systems Engineering*, Fourth Edition (eds P. Fortescue, G. Swinerd and J. Stark), John Wiley & Sons, Ltd, Chichester, UK. doi: 10.1002/9781119971009.ch9

[35] The Engineering Toolbox. "Emissivity Coefficients of Some Common Materials." Web. 12 Mar. 2012. [http://www.engineeringtoolbox.com/emissivity-coefficients-d\\_447.html](http://www.engineeringtoolbox.com/emissivity-coefficients-d_447.html)

[36] Dopart, C. et al. "Design and Analysis for a CubeSat Mission." MQP Report NAG-1102. Department of Mechanical Engineering, Worcester Polytechnic Institute, Worcester, MA, 2012.

[37] Dawson, E. et al. "Attitude Determination and Control System for a CubeSat Mission." MQP Report MAD - D11A. Department of Mechanical Engineering, Worcester Polytechnic Institute, Worcester, MA, 2012.

[38] Oliva, Andrew et al. "Design and Analysis of Subsystems for a CubeSat Mission" MQP Report NAG-1102. Department of Mechanical Engineering, Worcester Polytechnic Institute, Worcester, MA, 2011.